Physica 9D (1983) 1–32
North-Holland Publishing Company

RESONANCE STRUCTURE IN KINK–ANTIKINK INTERACTIONS IN ϕ^4 THEORY

David K. CAMPBELL†, Jonathan F. SCHONFELD††, and Charles A. WINGATE†

Received 29 November 1982

We present new numerical and theoretical results concerning kink–antikink collisions in the classical (nonintegrable) ϕ^4 field model in one-dimensional space. Earlier numerical studies of such collisions revealed that, over a small range of initial velocities, intervals of initial relative velocity for which the kink and antikink capture one another alternate with regions for which the interaction concludes with escape to infinite separation. We describe the results of a new high-precision computer simulation that significantly extends and refines these observations of escape "windows". We also discuss a simple theoretical mechanism that appears to account for this structure in a natural way. Our picture attributes the alternation phenomenon to a nonlinear resonance between the orbital frequency of the bound kink–antikink pair and the frequency of characteristic small oscillations of the field localized at the moving kink and antikink centers. Our numerical simulation also reveals long-lived small-scale oscillatory behavior in the time dependence of kink and antikink velocity following those collisions that do not lead to capture. We account for this fine structure in terms of the interaction between kink (and antikink) motion and small amplitude "radiation" generated during and after the collision. We discuss possible implications of our results for physical systems.

1. Introduction

Over the past several years it has become increasingly apparent that spatially localized, nonlinear excitations – "solitary waves" – contribute significantly to the behavior of a wide variety of natural systems, from organic polymers and biological structures through plasmas to quantized fields [1]. Yet, despite the clear importance and frequent analytic accessibility of these solitary wave excitations, their interactions, which can control many features of the dynamics of these systems, are in general poorly understood.

To be sure, in some cases systems can be modeled by equations in which the solitary waves are "solitons" in the strict sense [1, 2]. In these models, an infinite number of conservation laws lead to the complete integrability of the equations and so constrain the dynamics that these interactions are essentially trivial [1, 2]; solitons pass through each other with only a "phase shift" or "time delay" [1, 2] and the entire interaction can be described analytically. A celebrated example of this class of models, and one which we shall later use for comparison, is the sine-Gordon equation,

$$\frac{\partial^2 u(x,t)}{\partial t^2} - \frac{\partial^2 u(x,t)}{\partial x^2} + \sin u(x,t) = 0\,, \tag{1.1}$$

for which the static single kink (S) and anti-kink ($\bar{S}$) *soliton* solutions can be written as

$$u_S = 2\pi - u_{\bar{S}} = 4\tan^{-1}\{e^{(x-x_0)}\}\,. \tag{1.2}$$

More commonly, the underlying models do not contain strict solitons. Either there is some physical perturbation – a defect, an impurity, or a weak coupling to another system – which destroys the complete integrability, or the "bare" model itself is simply not integrable [3]. In these cases, interesting and highly nontrivial interactions can occur. Since

† Center for Nonlinear Studies and Theoretical and Theoretical Design Divisions, Los Alamos National Laboratory, Los Alamos, New Mexico 87545, USA.
†† Theoretical Department, Fermi National Accelerator Laboratory, P.O. Box 500, Batavia, Illinois 60510, USA.

0167-2789/83/0000–0000/$03.00

here one must typically resort to numerical simulations, it becomes both challenging and important to extract, at least qualitatively, the mechanisms underlying the observed interactions.

In this article we study the interactions of solitary waves in the non-integrable one-dimensional, classical ϕ^4 theory. This model is defined either by the Lagrangian density (whence the name ϕ^4)

$$\mathscr{L}(x,t)=\tfrac{1}{2}\left(\frac{\partial\phi}{\partial t}\right)^2-\tfrac{1}{2}\left(\frac{\partial\phi}{\partial x}\right)^2-\tfrac{1}{4}(\phi^2-1)^2\,, \qquad (1.3)$$

or by the resulting equation of motion

$$\frac{\partial^2\phi}{\partial t^2}-\frac{\partial^2\phi}{\partial x^2}-\phi+\phi^3=0\,. \qquad (1.4)$$

From either the Lagrangian density or the field equation, one can see that the conserved energy of the system is

$$E=\int \mathrm{d}x\left[\tfrac{1}{2}\left(\frac{\partial\phi}{\partial t}\right)^2+\tfrac{1}{2}\left(\frac{\partial\phi}{\partial x}\right)^2+\tfrac{1}{4}(\phi^2-1)^2\right]. \qquad (1.5)$$

Eq. (1.4) has static single kink (K) and anti-kink ($\bar{\mathrm{K}}$) solitary wave solutions of the forms

$$\phi_{\mathrm{K}(\bar{\mathrm{K}})}=\pm\tanh\left(\frac{x-x_0}{\sqrt{2}}\right), \qquad (1.6)$$

which are qualitatively very similar to the solitons of eq. (1.2). Indeed, in mathematical terms, both models are just nonlinear Klein–Gordon equations defined on the infinite line [4]. It is thus of interest to mathematics to understand the similarities and differences of these models.

Apart from this mathematical interest, the ϕ^4 model is of substantial interest in physics, where it arises in a number of applications. Historically, the first important use of the ϕ^4 theory (involving only the static limit) was in the Ginzburg–Landau phenomenological theory of second order phase transitions [5]. More recently, the one-dimensional ϕ^4 theory has been generally applied at a more microscopic level to structural phase transitions in the displacive limit [6–17] and specifically to uniaxial ferroelectrics [7–8, 11]. The role of the solitary waves in both the thermodynamics [9, 11, 15, 16] – where they appear as "fundamental" excitations in the partition function – and the dynamical response [7, 8, 10–17] – where they appear as mobile domain walls [10–17], leading to cluster formation [13, 14] and possibly explaining observed "central peak" phenomenon [8, 11–17] – has been extensively studied. A related but distinct application of the one-dimensional ϕ^4 model has been as a phenomenological theory of the nonlinear excitations in linear polymeric chains, such as polyacetylene [18, 19]. Here the kinks correspond to the nonlinear excitations having the celebrated exotic spin–charge relations [20]. In quantum field theory, the one-dimensional ϕ^4 model has been used as an example to illustrate the connection between nonlinear classical excitations and quantum particles [21]. Further, when coupled to fermions, it has been used as a "toy" model of nuclear physics [22] and as an illustration of the nontrivial effects of topology on fermion number [23]. Finally, higher dimensional versions of the ϕ^4 theory play a central role in the models of the spontaneous symmetry breakdown required in the unified theories of the electromagnetic and weak interactions [24].

Motivated by this combined mathematical and physical interest, a number of researchers [10, 25–32] have studied kink–antikink interactions in the ϕ^4 model numerically, using digital computers. All of them have reported that $\mathrm{K}\bar{\mathrm{K}}$ collisions with certain initial relative velocities end with kink and antikink reflecting from one another, while with other initial velocities the collisions end with $\mathrm{K}\bar{\mathrm{K}}$ capture into a bound state. Most surprisingly, most [10, 28, 29, 31, 32] of these authors have reported that there is *more than one* range of initial velocities for which the collisions end in reflection, and that these reflection regions alternate with more than one range of incoming velocities for which the collisions end in $\mathrm{K}\bar{\mathrm{K}}$ capture. To the best of our knowledge, there is no theoretical explanation, in the published literature, of this unexpected alternation pattern.

In this paper we present the results of a new, more extensive numerical study of $K\bar{K}$ collisions in the ϕ^4 model, and describe a semiphenomenological theory of the structure that we see. Numerically we confirm earlier claims, and we also observe many more, narrower, alternating regions of capture and reflection than hitherto reported. We also observe unanticipated fine structure in the time-dependence of the outgoing velocities of kinks and antikinks that leave interactions ending with $K\bar{K}$ reflection. Our theory accounts qualitatively for all our observations.

In section 2, after beginning with some elementary remarks contrasting kink interactions in the sine-Gordon and ϕ^4 theories, we describe in detail the most significant results of our numerical simulations and the ingredients in, and predictions of, our semi-phenomenological theory. In section 3 we present the detailed justification of this theory. Section 4 describes and explains the fine structure, mentioned above, in the outgoing velocity of kinks and antikinks leaving interactions. In section 5 we conclude with some remarks on both the limitations and the generality of our approach and indicate briefly possible implications for real physical systems. In appendix A we present the details of our numerical scheme and in appendix B we include some calculational and conceptual background for our analytic results.

2. Qualitative discussion and overview of results

Before discussing the more intricate details of ϕ^4 kink collisions, it is useful to begin with a few elementary remarks comparing and contrasting these interactions with those of the sine-Gordon solitons. In the sine-Gordon theory, the interaction of a soliton (S) and anti-soliton ($\bar{S}$) is described in their center of mass system by the analytic function [2, 33]

$$u_{S\bar{S}} = 4\tan^{-1}\left\{\frac{\sinh(vt/\sqrt{1-v^2})}{v\cosh(x/\sqrt{1-v^2})}\right\}. \tag{2.1}$$

In fig. 1 we present qualitative sketches of this function at different times. For large negative time (fig. 1a) $t = -T$, the S and $\bar{S}$ are widely separated ($\Delta x \approx 2(vT - \sqrt{1-v^2}\ln v)$ but approaching each other ($v_S = -v$, $v_{\bar{S}} = +v$). For $t \approx 0$ (figs. 1b and 1c) they interact in a highly nonlinear manner that nonetheless permits them to pass through each other "unscathed". For $t = +T'$ (fig. 1d) they are separating with final velocities equal to their initial velocities; the only effect is a small shift in the position that they would have reached had there been no interaction.

This "phase shift" or "time delay" can be shown, from (2.1), to be

$$\delta x = 2(1-v^2)^{1/2}\ln(1/v)\,. \tag{2.2}$$

Note that when the S and $\bar{S}$ pass through each other, the region near $x = 0$ is left in the "ground state" with $u = 2\pi$, whereas before the interaction it was at $u = 0$. This is possible because of the $u \to u + 2\pi n$ symmetry of eq. (1.1).

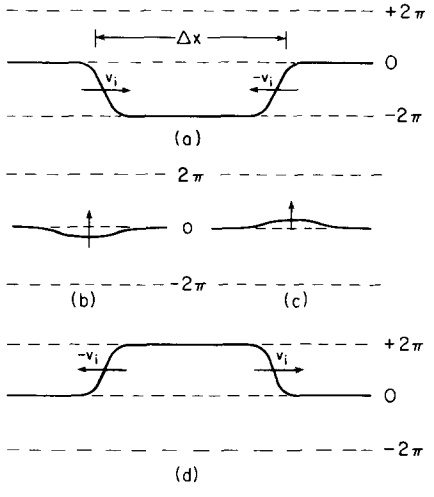

Fig. 1. A schematic depiction of the interaction of a soliton (S) and an antisoliton ($\bar{S}$) in the sine-Gordon equation. (a) The initial condition, at $t = -T$; (b) and (c) the field configurations at $t = -\epsilon$ and $t = +\epsilon$, respectively ($\epsilon \approx 0$); (d) the final field configuration at $t = +T'$. Note that when the S and $\bar{S}$ pass through each other, the region near $x = 0$ is left in the ground state with $u = 2\pi$ instead of $u = 0$.

In the case of ϕ^4 interactions, we have no analytic guidance, and hence in fig. 2 we sketch (again, qualitatively) several a priori possible results of K$\bar{\text{K}}$ collisions. Fig. 2a shows the initial state, with $\bar{\text{K}}$ and K approaching each other in their center of mass system. The configuration in fig. 2b, in which the $\bar{\text{K}}$ and K appear to have passed through each other, is in fact impossible on energetic grounds alone. Since the region between the kinks is at some value ϕ_0 *not* equal to a minimum of the potential, the energy of this configuration is $E \approx V(\phi_0)L$, and hence L can *not* approach infinity. To reiterate: in the ϕ^4 theory, K and $\bar{\text{K}}$ can not pass through each other [34]. Fig. 2c shows a possible final state in which the K and $\bar{\text{K}}$ have *reflected* from each other. Anticipating the nonintegrable nature of the theory, we have indicated that $v_f \neq v_i$ [34]. In fig. 2d we indicate the possibility that the $\bar{\text{K}}$ and K "annihilate" almost immediately in the collision, sending out dispersing "radiation" ("phonons", in the solid state terminology). Finally, in fig. 2e we sketch a "final state" in which a long-lived, spatially localized, time-oscillatory state is formed; this state may decay in time by emitting "radiation".

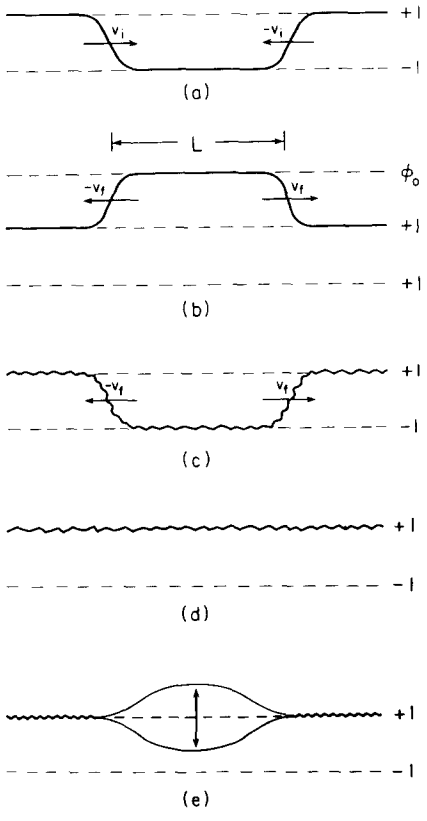

Fig. 2. A schematic depiction of "possible" results of kink (K) and antikink ($\bar{\text{K}}$) collisions in ϕ^4 theory. (a) The initial state, $t = -T$; (b) a putative final state in which the K and $\bar{\text{K}}$ pass through each other. This state has energy $E \propto V(\phi_0)L$ and hence, as argued in the text, $L \nrightarrow \infty$, and it cannot be an asymptotic state of the system: (c) a final state in which the K and $\bar{\text{K}}$ reflect, presumably inelastically ($v_f \neq v_i$); (d) a putative final state in which the K and $\bar{\text{K}}$ have annihilated rapidly to produce dispersing "radiation"; (e) a "final" state containing a spatially localized, time oscilatory motion plus small radiation. This state is very long-lived, but decays eventually into radiation.

In principle, the behaviors sketched in figs. 2c–2e are all possible. In practice, our numerical simulations, consistent with earlier results [25–32], show that only possibilities of fig. 2c and 2e are observed. This is perhaps intuitive physically, for it indicates that ϕ^4 kinks retain some of the robustness of their sine-Gordon cousins. Further, by analogy to the relation between the sine-Gordon breathers and the S and $\bar{\text{S}}$ solitons, the localized oscillatory state in fig. 2e can be thought of as a $\bar{\text{K}}$ + K bound state [25–28], in which the kinks are trapped by their mutual attraction [25, 30, 32]. Since the trapped state can be formed only if the kinks have time to lose sufficient energy in a collision, one expects trapping at low relative velocity, and (inelastic) reflection at high v_i.

The full results of our numerical simulations are summarized in fig. 3 for the range $0.16 \leqslant v_i \leqslant 0.4$. In this plot, $v_f = 0$ implies that no kinks exist in the asymptotic state; instead, a "trapped" oscillatory state is formed. As anticipated, at low initial velocities ($v_i < 0.193\ldots$) a trapped state is always formed, and at high velocities ($v_i > v_c = 0.2598\ldots$) the kinks always reflect inelastically. The striking feature of fig. 3 is the sequence of regions of intermediate v_i in which trapping and reflection alternate. For definiteness, let us call these regions below v_c in which reflection occurs "reflection windows". A catalogue of the "reflection win-

Table I
A tabulation of the range, center, and width in initial velocity of the reflection windows observed in ϕ^4 K$\bar{\text{K}}$ collisions. The last three columns give respectively, the theoretically predicted value of the window center and two quantities which our theory predicts to be constant. In the last two columns v = center of window and Δv = width

$N_w = n - 2$	Range of v	Center	Width	Predicted Center	$(v_c^2 - v^2)(2n+1)^2$	$\Delta v(2n+1)^3$
1	0.1926 – 0.2034	0.1980	0.0109	0.1990	1.39	3.74
2	0.2241 – 0.2288	0.2265	0.0048	0.2250	1.31	3.50
3	0.2372 – 0.2396	0.2384	0.0025	0.2370	1.29	3.33
4	0.2440 – 0.2454	0.2447	0.0015	0.2437	1.29	3.30
5	0.2481 – 0.2490	0.24855	0.0010	0.2478	1.29	3.38
6	0.2507 – 0.2513	0.2510	0.0007	0.2505	1.30	3.44
7	0.2525 – 0.2529	0.2527	0.0005	0.2524	1.31	3.4
8	0.2538 – 0.2541	0.25395	0.0004	0.2538	1.33	3.7
9	0.2548 – 0.2550	0.2549	0.0003	0.2548	1.33	4.3

dows" observed in our numerical simulations is shown in table I*.

The existence of a threshold above which the kink and antikink always reflect has been known numerically [10, 25–32] and understood semi-quantitatively [30] for some time. Further, the lowest three "windows" in the table have been observed in earlier work [10, 25, 27–29, 31–32], but no explanation of the origin of these "resonance windows" has been proposed. In the remainder of this article we shall focus on this resonance structure, presenting further results of computer calculations and formulating a simple, semi-phenomenological theory that is in good agreement with the numerical observations. We begin by describing here the ingredients in our theoretical approach and their relation to our numerical results.

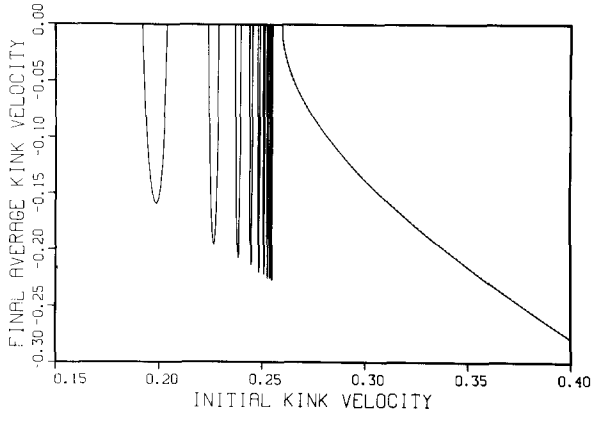

Fig. 3. The (time-averaged – see section 4) kink velocity (solid curve) after a K$\bar{\text{K}}$ collision as a function of the initial kink velocity. A final velocity of zero means K$\bar{\text{K}}$ capture into a bound state. The dashed curve (which is almost indistinguishable from the data) is a fit to the form (constant) $\times (v^2 - v_c^2)^{1/2}$ for v above and close to v_c.

The first important ingredient is the observation that there is a crucial distinction between K$\bar{\text{K}}$ reflections above v_c and those in the "resonance windows" below v_c. Specifically, as shown in fig. 4, above v_c the K and $\bar{\text{K}}$ collide once and then reflect to infinity, whereas in the windows below v_c the K and $\bar{\text{K}}$ collide, recede to finite separation, stop, and

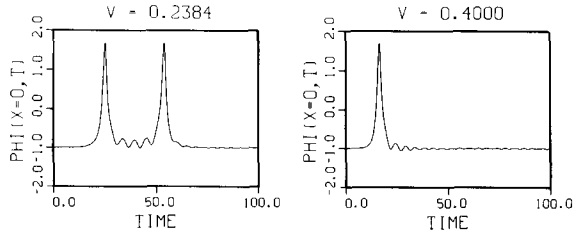

Fig. 4. $\phi(x = 0, t)$ versus t for K$\bar{\text{K}}$ collisions (a) in a "two bounce resonance window" below v_c and (b) above $v_c = 0.2598$.

* A natural reaction to first seeing this table is to wonder whether the resonances continue indefinitely, clustering toward v_c as $n \to \infty$. In its most naive form, the theory we describe below would predict this, but as we discuss later there are a number of effects not included in the naive theory that can cause the sequence to terminate.

then return to collide again before reflecting to infinity [28, 32]. Thus we shall henceforth use the term "two-bounce windows" to refer to these reflection resonances. Before the first collision and during most of the time between the two bounces the K and $\bar{\text{K}}$ exist as separate entities. Hence it is sensible to speak of a potential energy [25, 30, 32] (or force) between them (see appendix B) and of the kinetic energy of the translational motion of each kink. The "two bounce" behavior indicates (1) that after the first collision the K and $\bar{\text{K}}$ are trapped by their attractive potential and hence that energy has been removed from their translational motion, but also (2) that after the second collision, this energy is at least in part restored, allowing the kinks to escape. To explain this behavior one clearly needs a mechanism for transferring and storing energy. In view of the separation of the K and $\bar{\text{K}}$ between bounces, it is natural to look for the mechanism in the small oscillations around a single kink (or antikink). These small oscillations, $\delta\phi$, are determined by the equation

$$\frac{\partial^2\delta\phi}{\partial t^2} - \frac{\partial^2\delta\phi}{\partial x^2} + (3\phi^2_{\text{K}(\bar{\text{K}})} - 1)\delta\phi = 0\,. \tag{2.3}$$

Fourier transforming with respect to time, one can convert this to a Schrödinger equation with potential [using (1.6)],

$$V_{\text{SCH}}(x)5 \equiv (3\phi^2_{\text{K}(\bar{\text{K}})} - 1) = 2 - 3\,\text{sech}^2\frac{(x - x_0)}{\sqrt{2}}\,, \tag{2.4}$$

which corresponds to a well-known solvable (in fact, reflectionless) potential [30, 35, 37]. In terms of the Fourier transform variable ω, the spectrum of (2.3) has a continuum beginning at angular frequency $\omega_c = \sqrt{2}$ and two normalizable modes, with angular frequencies $\omega = 0$ and $\omega = \omega_s = \sqrt{3/2}$. The continuum corresponds physically to dispersive travelling waves that propogate to spatial infinity. The zero frequency mode, whose wave function, $\delta\phi_0$, is proportional to the spatial derivative of $\phi_{\text{K}(\bar{\text{K}})}$, corresponds to the translation of the kink (antikink). The mode with $\omega_s = \sqrt{3/2}$ represents a localized deformation around the kink and can be considered physically as an internal shape mode oscillation of the kink. The normalized eigenfunction of the "shape mode" is

$$\delta\phi_s \equiv 2^{-3/4}\tanh\frac{x - x_0}{\sqrt{2}}\,\text{sech}\frac{x - x_0}{\sqrt{2}}\,. \tag{2.5}$$

Since it is localized about the kink, this shape mode is the natural candidate for the degree of freedom in which to store the translation energy of the trapped K and $\bar{\text{K}}$ in a two-bounce wirdow. This hypothesis is further supported by the analysis of Sugiyama [30], who, assuming that most of the kinetic energy lost in the initial K + $\bar{\text{K}}$ collision is transferred to the shape mode, estimated the critical velocity for the first capture to be $v_c \approx 0.25$, in very good agreement with the actual $v_c = 0.2598\ldots$*. If we adopt this hypothesis, then because of the time-reversal invariance of eq. (1.4), we may also conclude that if the initial state consists of an internally vibrating kink and an internally vibrating antikink, and if the amplitudes of vibration are chosen judiciously, and if the phases of the initial internal vibrations are synchronized properly with the time of impact, then the effect of a collision can be to extinguish all shape oscillations, with a concomitant increase in K$\bar{\text{K}}$ kinetic energy.

We claim that the second, liberating reflection of a kink and antikink whose initial speeds are in a two-bounce window is an example of this reverse process. The first reflection sets up shape oscillations which carry more energy† than the kinetic energy of the original asymptotically separated K and $\bar{\text{K}}$, so that the kink and antikink after the first collision are bound; the second collision extinguishes the shape vibrations, when the timing is right, restoring enough of the lost kinetic energy

* We will discuss the distribution of energy among the various modes in more detail in the later sections. See also fig. 9.

† Recall that, because of the attractive potential, as the kinks approach each other, they gain kinetic energy.

that the $K\bar{K}$ are again unbound. Favorable timing in this case means that the occasion of the second impact coincides with the passage of the internal vibration through some phase angle characteristic of shape-mode extinction. Thus, the condition for restoration of $K\bar{K}$ kinetic energy after the second bounce ought to be of the form

$$\omega_s T = \delta + 2\pi n\,, \tag{2.6}$$

where T is the time between the first and second impact, δ is some offset phase, and n is an integer.

Fig. 5 shows, in the points marked "X", the time between the two bounces of a kink and antikink with initial speed at the center of a two-bounce window, versus the ordinal number of the first nine windows (plus two, in order to get δ between zero and 2π). These correspond to the entries in table I, reading downward. This figure also shows a straight line that passes through all the nine marks. The slope of the line is 5.2, which compares well with the value $2\pi/\omega_s = 2\pi\sqrt{2/3} \approx 5.13$, expected from (2.6). From the intercept of this line, the phase δ is 3.3 ($\approx \pi$).

The validity of the linear relation (2.6) is more dramatically illustrated in the sequences of pictures in fig. 6, showing graphs of $\phi(x, t)$ at $x = 0$ as a function of time for collisions whose initial $K\bar{K}$ speeds are at the centers of the first eight of our nine resolved two-bounce windows. As in fig. 4, the two large spikes in each picture correspond to the two $K\bar{K}$ reflections, while the bumps between the spikes correspond* to the sum of the tails of the shape oscillation waveforms centered on the kink and antikink. According to formula (2.6), one expects that each picture in fig. 6 should have one more bump in it than in the preceding one, and this is indeed what one sees.

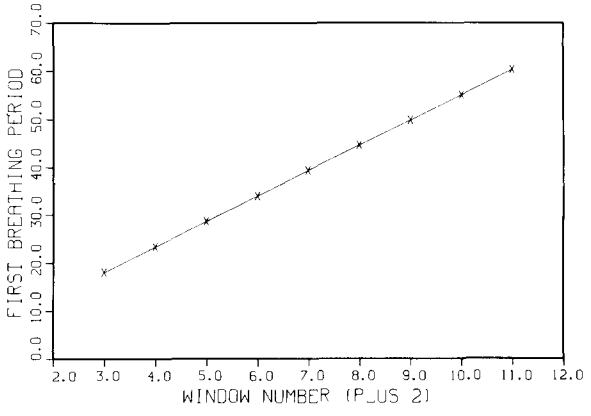

Fig. 5. The time between the first and second $K\bar{K}$ impacts for incoming speeds at the centers of the two-bounce windows as a function of the window number (points marked "X"). The straight line is a linear fit.

Although we cannot account quantitatively for the fact that we see no window corresponding to n less than three in (2.6), the existence of some nontrivial lower limit on n is not unreasonable. Presumably, when the interval between bounces is $\omega_s^{-1}(\delta + 4\pi)$ and lower, the kinks do not have time to separate far enough to form well-defined shape oscillations and therefore resonance cannot occur.

The second ingredient in our theory is a relation between the observed time between bounces and the initial velocity of the kinks. In section 3 we shall present heuristic arguments suggesting that for $K\bar{K}$ initial speeds v just below v_c, the time between the first two impacts of the kink and antikink should satisfy

$$T(v) \propto (v_c^2 - v^2)^{-1/2}\,. \tag{2.7}$$

Although we can not rigorously prove this result – hence the "semi-phenomonological" nature of our theory – it is in excellent agreement with our numerical results (fig. 7), except that the naively predicted proportionality constant, (≈ 2.4) is lower than the value (≈ 3.0) found from the numerical results. Using the number from the simulation (3.0), eq. (2.7) then implies that the window centers are located at

$$v_n^2 = v_c^2 - \frac{1.37}{(2n + \delta/\pi)^2} \approx v_c^2 - \frac{1.37}{(2n+1)^2}\,. \tag{2.8}$$

* We provide a more explicit discussion of this is section 3. Here we note simply that the structure has the correct period, $2\pi/\omega_s \approx 5.1$.

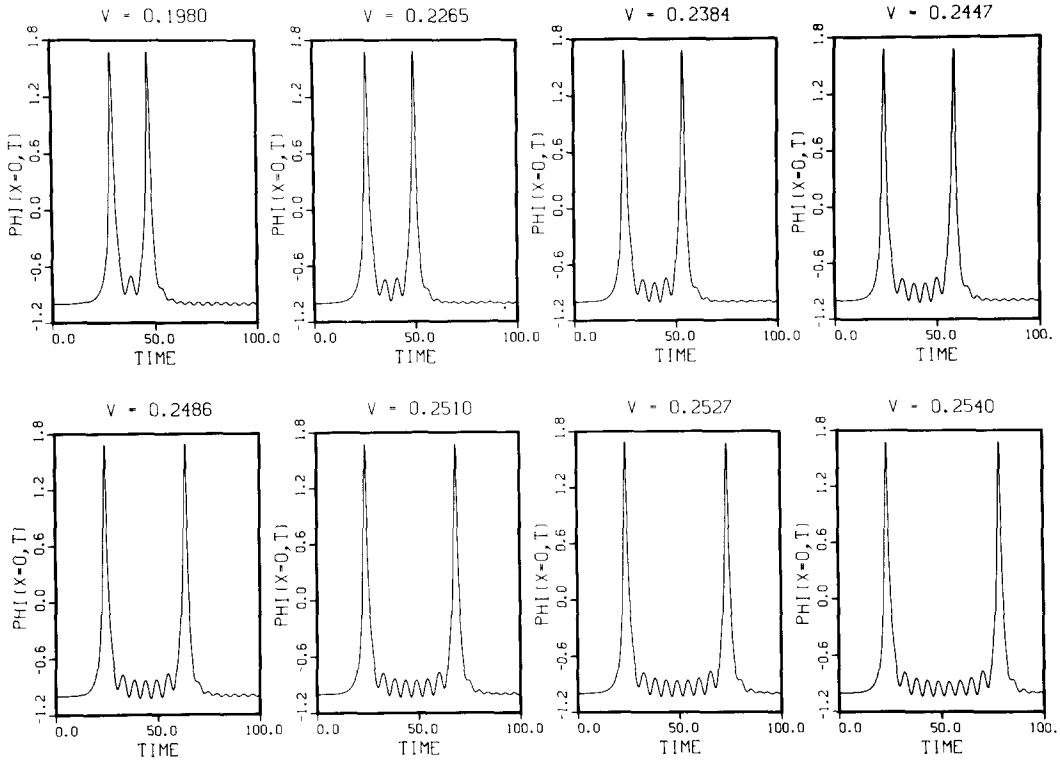

Fig. 6. $\phi(x = 0, t)$ versus t for incoming speeds at the centers of the first eight two-bounce windows.

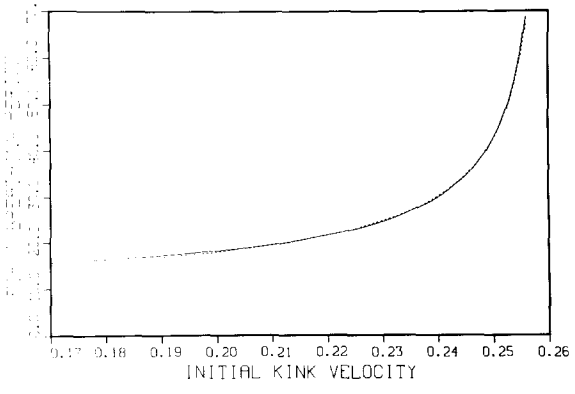

Fig. 7. The time $[T(v)]$ between the first and second $K\bar{K}$ impacts as a function of the incoming speed $v < v_c$ (solid curve). The dashed curve is a fit to (constant)/$\sqrt{v_c^2 - v^2}$.

Eq. (2.8) shows that $(v_c^2 - v_n^2)(2n + 1)^2 = 1.37$, a constant for all n. This compares well with the figures in the sixth column of table I, which are the different values of $(v_c^2 - v_n^2)(2n + 1)^2$, as determined directly from the numerical data figures in the first and third columns.

Our resonance picture also enables us to understand, in a semiquantitative way, the window widths. In particular, since the resonance condition (2.6) indicates that the process of transfer of shape-mode energy back to $K\bar{K}$ kinetic energy is largely independent of how many shape oscillations have preceded the second $K\bar{K}$ impact, we expect that the window width in velocity is determined by an angular width in shape-mode phase: that is,

$$\omega_s \Delta T = \theta\,, \tag{2.9}$$

with some constant (i.e., n-independent) θ. Setting $\Delta T = (\partial T/\partial v)\Delta v$, and using (2.7) with proportionality constant 3.0 gives

$$\Delta v_n \approx (1.7)\theta/(2n + 1)^3\,. \tag{2.10}$$

Comparing with the seventh column in table I, we see that (2.10) is in reasonable agreement with the numerical results provided $\theta \approx 2.0$. This is consistent with a theoretical estimate $\theta \lesssim 2$, which we shall derive in section 3.

Before turning to the detailed derivations of our central results, we pause to discuss some obvious points raised by this qualitative discussion. First, there is no reason a priori that n-bounce windows ($n > 2$), corresponding to initial speeds for which the "instant" of the nth $K\bar{K}$ collision coincides with the passage of the shape oscillation through the proper phase, should not exist. Since this was not observed in the data summarized in table I, we shall not discuss here the (obvious but technically complicated) generalization of our resonance approach to this case [37]. Second, the version of the resonance theory* sketched here implies the existence of an infinite sequence of increasingly narrow windows as $v \to v_c$ from below. In fact, this version ignores entirely the effects of the continuum modes – "radiation" – in the expansion around the K and $\bar{K}$. These modes are excited at some level both at the "instants" of collision and as the translating and oscillating kinks move back and forth between collisions. Since this radiation disperses to infinity, for very long intercollision times – that is, by (2.7), for the putative windows with very large n – the radiation would be expected to degrade the shape mode to the point that there is not enough energy available at the time of the second impact to unbind the $K\bar{K}$ pair. Thus there should be an upper limit on the n observed in two-bounce windows, although we shall not estimate it here.

That the radiation, although small, can play an important role in the $K\bar{K}$ interaction is also shown by some fine structure effects that we have observed both in the outgoing kink speed and in the behavior of $\phi(0, t)$ versus time. These effects, which are discussed in detail in section 4, can only be explained by careful consideration of the coupling to radiation.

* A natural reaction to first seeing this table is to wonder whether the resonances continue indefinitely, clustering toward v_c as $n \to \infty$. In its most naive form, the theory we describe below would predict this, but as we discuss later there are a number of effects not included in the naive theory that can cause the sequence to terminate.

3. Quantitative theory of the "two bounce" resonance windows

3.1. *Time between the two kink–antikink interactions*

The solitary, "particle-like" nature of the ϕ^4 kinks has led a number of authors [25, 30, 32] to propose a phenomenological potential to describe nonrelativistic, elastic, $K\bar{K}$ interactions. This potential, $V(x_0)$, which is a function of the kink–antikink separation, is obtained by substituting the Ansatz function ϕ_A

$$\phi_A \equiv \phi_K(x - x_0) + \phi_{\bar{K}}(x + x_0) + 1 \tag{3.1}$$

into the energy integral (1.5). Thus the potential represents the energy of a field configuration consisting, at least for large x_0, of a clearly defined, static, kink–antikink pair at separation $2x_0$. To describe motion in the system, it is natural (see also appendix B) to allow x_0 in (3.1) to become time dependent and to insert this time-dependent Ansatz into (1.5) to obtain an effective Hamiltonian for $x_0(t)$. The result is

$$H = M\dot{x}_0^2 + I(x_0)\dot{x}_0^2 + V(x_0)\,, \tag{3.2}$$

where M is the kink rest mass and the explicit forms of $I(x_0)$ and $V(x_0)$ [30, 32] are, for completeness, given in appendix B. For large positive x_0, $I(x_0) \to 0$† and $V(x_0)$ takes the form, when the constant $V(\infty) = 2M$ is subtracted,

$$\tilde{V}(x_0) = V(x_0) - 2M \approx -12M \exp(-2\sqrt{2}x_0)\,. \tag{3.3}$$

†Since $I(x_0)$, like $V(x_0)$, falls off exponentially, it might appear that we should include its effect in the asymptotic energy balance equation determining $T(\epsilon)$. This effect is small, however, since the leading coefficient of $\dot{x}_0^2$ is the constant M, and thus we can ignore this inessential complication.

As might have been expected, this is a static Yukawa potential. Recalling that the K$\bar{\text{K}}$ separation is $2x_0$, we see that the range of this potential is given by one over the "mass" of the travelling wave continuum, $m = \omega_c = \sqrt{2}$.

To describe the motion of the bound K$\bar{\text{K}}$ pair *between* the two bounces, we shall assume, as a first approximation, that the energy expression in (3.2) is conserved and, since this system is weakly bound, that the total energy is $-M\epsilon$, where $\epsilon \ll 1$. We shall use this to determine $T(\epsilon)$, the time between bounces as a function of ϵ. When this is done, we shall relate ϵ to the initial kink and antikink velocities so that we will finally have $T(v)$.

Before presenting this determination, let us comment on several aspects of this effective Hamiltonian approach. First, the decomposition (3.1) is simplistic at small x_0, where the kink and antikink overlap and lose their identity. This is not a big problem for determining $T(\epsilon)$ because for v near v_c the K$\bar{\text{K}}$ configuration formed after the first impact is very weakly bound, so that the kink and antikink spend most of the time between their "collisions" at large x_0, near the outside orbital turning points. This means that the small-x_0 behavior of the potential does not contribute to the leading behavior of $T(\epsilon)$ and also that the term involving $I(x_0)$ can be neglected.* Second, when the shape modes are excited, one expects them to induce an additional K$\bar{\text{K}}$ interaction with range determined by the shape eigenfunction (2.5). Even if the shape mode amplitudes are small, this induced interaction might not be negligible, compared to the effects of $V(x_0)$, because the range of $\delta\phi$, which is $\sqrt{2}$, is longer by a factor of two than the range of $V(x_0)$ (in terms of $2x_0$), which is $1/\sqrt{2}$. Third, the nonlinear nature of the equation leads to coupling among all the modes – translation, shape, and radiation – which invalidates assumption of conservative translational motion. However, for small shape mode amplitudes and weak binding, this effect should be small.

Let us now proceed to estimate the leading behavior of $T(\epsilon)$, for small ϵ, from eq. (3.2). Setting the total energy in (3.2) equally to $2M - M\epsilon$ and neglecting the (nonleading) term involving $I(x_0)$* yields

$$M\dot{x}_0^2 + V(x_0) = 2M - M\epsilon\,. \tag{3.4}$$

Solving for the time between bounces in the usual way gives

$$T(\epsilon) = 2\int \frac{\mathrm{d}x}{\sqrt{-\epsilon - M^{-1}\tilde{V}(x_0)}}\,, \tag{3.5}$$

where the suppressed lower and upper limits on the integral correspond to the inner and outer turning points of the orbit. The outer turning point depends sensitively on ϵ for ϵ small, because $\tilde{V}(x_0)$ goes to zero for large x_0. In contrast the inner turning point is relatively insensitive to small ϵ. Thus, for $\epsilon \ll 1$, we may approximate (3.5) by

$$T(\epsilon) \approx T_0 + 2\int_{(x_0)_{\min}}^{(-1/2\sqrt{2})\log(\epsilon/12)} \frac{\mathrm{d}x_0}{\sqrt{12\,\mathrm{e}^{-2\sqrt{2}x_0} - \epsilon}}\,, \tag{3.6}$$

where $(x_0)_{\min}$ and T_0 are ϵ-independent constants. The integral in (3.6) is elementary, with the result

$$T(\epsilon) \approx T_0 + \frac{\sqrt{2}}{\sqrt{\epsilon}}\tan^{-1}\left(\frac{12\,\mathrm{e}^{-2\sqrt{2}(x_0)_{\min}}}{\epsilon} - 1\right)^{1/2} \underset{\epsilon\to 0}{\simeq} \frac{\pi}{\sqrt{2\epsilon}} + \mathcal{O}(\epsilon^0)\,. \tag{3.7}$$

We next need to relate the amount by which the kinks are bound, $-M\epsilon$, to their common initial velocity, v, in the region in which v is slightly less than v_c. We shall first present a heuristic argument suggesting the analytic form of the relation and then show that the resulting form for $T(v)$ is remarkably consistent with our data. Since we can not rigorously derive the form of $T(v)$, we shall refer to our theory as "semi-phenomenological".

* Since $I(x_0)$, like $V(x_0)$ falls off exponentially, it might appear that we should include its effect in the asymptotic energy balance equation determining $T(\epsilon)$. This effect is small, however, since the leading coefficient of $\dot{x}_0^2$ is the constant M, and thus we can ignore this inessential complication.

In the initial kink–antikink collision, energy is lost from the kinetic energy of the kinks both to the shape mode oscillations and to radiation modes. Let use call the total energy in these modes $\delta E(v)$. We shall assume that for v near v_c, this energy and consequently the energy lost are smooth, slowly-varying functions of the available kinetic energy ($\propto v^2$). For $v < v_c$, the energy lost determines the binding energy according to

$$\delta E(v) - Mv^2 = M\epsilon, \quad v < v_c, \tag{3.8a}$$

whereas for $v > v_c$, the energy lost determines the outgoing kink speed (v_f) according to

$$\delta E(v) - Mv^2 = -Mv_f^2, \quad v > v_c. \tag{3.8b}$$

The assumption of smooth variation of δE implies a smooth continuation between the binding energy (for $v < v_c$) and the outgoing kink speed for $v > v_c$. We shall use this later to check our heuristic results. Since $\epsilon = 0$ at $v = v_c$,

$$\delta E(v_c) = Mv_c^2 \tag{3.9a}$$

and thus, for v near v_c, we expect

$$\delta E(v) = Mv_c^2 + b(v^2 - v_c^2) + \cdots. \tag{3.9b}$$

We expect $b > 0$, since for smaller v (and hence smaller available energy) we expect overall a smaller transfer of energy. Substituting (3.9b) into (3.8a) yields

$$\begin{aligned}\epsilon &= (1 - b/M)(v_c^2 - v^2), \quad \text{for } v < v_c \\ &\equiv \alpha(v_c^2 - v^2),\end{aligned} \tag{3.10a}$$

with $\alpha = 1 - b/M$, whereas substituting into (3.8b) yields

$$v_f^2 = \alpha(v^2 - v_c^2), \quad \text{for } v > v_c. \tag{3.10b}$$

As a first check, we can compare eq. (3.10b) to our numerical data. Fig. 3 shows the outgoing kink velocity (v_f) as a function of the incoming kink velocity, v, for $v > v_c$. For v close to v_c, this curve is well described by the form

$$v_f^2 = \alpha(v^2 - v_c^2), \tag{3.11}$$

with $\alpha \approx 0.84$, indicating that $b/M = 0.16$. Using (3.10a) this means

$$\epsilon \approx \alpha(v_c^2 - v^2), \quad \text{with } \alpha = 0.84 \tag{3.12}$$

for $v < v_c$; and therefore, by (3.7)

$$T(v) \approx \frac{\pi}{\sqrt{2\alpha(v_c^2 - v^2)}} \approx \frac{2.4}{\sqrt{v_c^2 - v^2}}. \tag{3.13}$$

As indicated in section 2, this agrees in shape with the results of the numerical simulation shown in fig. 7, although the numerical data favors the proportionality constant 3.0. This 20% agreement is encouraging, for it indicates that we can understand semi-quantitatively the observed dependence of T on the initial velocity. Note that for the resonance theory we must use the *actual* time between collisions, and hence we take the form of (3.13) with the empirical constant 3.0. This leads to the remarkable quantitative agreement of theory and experiment shown in table I.

Before proceeding to our theory of θ, let us show how to use the notions introduced in this subsection to account in a rough way for the size of the oscillations bounded by the spikes in the pictures of fig. 6.

We shall try to estimate the amplitude of these oscillations by first estimating the amplitude of shape oscillations and then multiplying twice this amplitude (for the contributions of both kink and antikink) by the normalized wavefunction of (2.5), evaluated for x equal the maximum distance from kink to origin during the corresponding bound $K\bar{K}$ orbit. This choice is motivated by recalling that, as we remarked previously, the kink and antikink spend most of the time between collisions near this maximum separation. This maximum distance will be determined by the outer turning point of (3.5), with ϵ given by (3.12).

First, to estimate shape-mode amplitudes, we define the shape-mode amplitude S by writing the shape-oscillation as $(Se^{i\omega_s t} + S^* e^{-i\omega_s t})\delta\phi_S$. With this normalization, the energy in the kink's shape oscillation is $2|S|^2\omega_s^2$ and the total of that in the shape oscillations of both kink and antikink is $4|S|^2\omega_s^2$, since all collisions studied numerically are symmetric under spatial reflection and hence give rise to an outgoing kink and antikink that vibrate as mirror images. Since, to a first approximation (see next subsection), most of the initial $K\bar{K}$ kinetic energy ($\approx Mv_c^2$ for v near v_c) is transferred, on first impact, to shape oscillation, we may set

$$4|S|^2\omega_s^2 \approx Mv_c^2 , \tag{3.14}$$

This gives $|S| \approx 0.1$. The maximum value of the coordinate x_0 for a bound $K\bar{K}$ orbit of binding energy $M\epsilon$ satisfies, according to (3.2) and (3.3),

$$\exp(-2\sqrt{2}x_0) = \epsilon/12 . \tag{3.15}$$

Thus, according to (2.5) the value of $\delta\phi_S$ evaluated at this coordinate is approximately

$$\delta\phi_S(y) \approx 2^{1/4} e^{-x_0/\sqrt{2}} = 2^{1/4}\left(\frac{\epsilon}{12}\right)^{1/4} \approx \left(\frac{\alpha}{6}\right)^{1/4}(v_c^2 - v^2)^{1/4} . \tag{3.16}$$

To make the estimate, we use the result $\alpha \approx 0.84$ and find that (3.16) is between about 0.3 (for $v = 0.198$) and about 0.1 (for $v = 0.254$).

Thus the combined total of the two shape-mode tails at $x = 0$ is estimated roughly to be

$$2 \times 0.2 \times 0.2 \times \cos(\text{phase} + \omega_s t) \approx (0.1)\cos(\omega_s t + \text{phase}) , \tag{3.17}$$

in all pictures, which is what one observes.

3.2. *The energy in the shape modes and the width of the resonance windows*

We first derive in this subsection an approximate expression for the energy in shape oscillation after two $K\bar{K}$ reflections, as a function of the time between the bounces. We shall make the simplifying assumptions that no radiation is emitted in the process, and that the effect of a $K\bar{K}$ collision on the shape oscillations occurs completely and instantaneously, at the moment of impact (to the extent that such a moment can be defined). The second assumption allows us to neglect the time-dependence of the energy in shape oscillations between collisions, and the first assumption allows us to determine the window boundaries – and therefore window widths – by setting the shape mode energy, after two bounces, equal to the initial $K\bar{K}$ kinetic energy. This signifies that after the second bounce, the kink and antikink are just barely unbound.

Since the shape mode amplitudes are small in this context, we shall also suppose in what follows that there is an approximately linear relation between the amplitudes of internal vibration of the $K\bar{K}$ leaving a collision and the amplitudes of internal vibration of the incoming kink and antikink. In particular, let S represent the complex amplitude of kink shape oscillation before a collision (assumed to take place at $t = 0$). Thus, as in the preceding subsection, before the collision the kink shape oscillation is $(S e^{i\omega_s t} + S^* e^{-i\omega_s t})\delta\phi_S$. We stress again that it is not necessary to introduce a separate notation for shape oscillation of an antikink, since in the spatially symmetric collisions that we simulate numerically, kink and antikink vibrate as mirror images. Let S' represent the complex shape mode amplitude after the collision. Then we suppose there are complex parameters a, $\tilde{a}$, and ρ such that

$$S' \approx aS + \tilde{a}S^* + \rho . \tag{3.18a}$$

Observe that if the collision takes place at time T instead of at time zero, (3.18a) is modified to read

$$S' \approx aS + \tilde{a}S^* e^{-2i\omega_s T} + \rho e^{-i\omega_s T} . \tag{3.18b}$$

A priori, a, $\tilde{a}$, and ρ can depend on the kink velocity (or initial $K\bar{K}$ binding energy) preceding

the collision. However, inasmuch as the window phenomenon occurs in a small region of v, in which the velocities and binding energies are both small, we shall, in what follows, neglect the dependence of a, $\tilde{a}$, and ρ on pre- (or post-) collision conditions.

Since the initial conditions of our simulated $K\bar{K}$ collisions never have any shape oscillation excited, our numerical results give as direct information about ρ. In particular, energetics (i.e., the fact that shape-mode formation extinguishes kink and antikink translational motion at $v = v_c$) implies that (as already argued in the preceding subsection)

$$Mv_c^2 \approx 4\omega_s^2|\rho|^2 , \tag{3.19}$$

so that $|\rho| \approx 0.1$. Also, the timing of the crests and troughs in the pictures of fig. 6 gives

$$\operatorname{Arg}\rho \approx -\pi/2 . \tag{3.20}$$

The coefficients a and $\tilde{a}$ cannot be determined from our data in a similarly direct way. We describe below an indirect way of constraining these parameters. When this is done we will be able to compute the amplitude of shape oscillation after two $K\bar{K}$ impacts by successively applying transformations (3.18a) and (3.18b), with T equal to the time between impacts.

To obtain information about a and $\tilde{a}$, we exploit the time-reversal invariance of the original equation of motion (1.4). Time reversal interchanges the amplitudes S and S'^*. Thus, if (3.18a) is to be an acceptable condensation of the time-symmetric (1.4), we should have, for all S,

$$\begin{aligned} S^* = (S'^*)' &= aS'^* + \tilde{a}S' + \rho \\ &= (|a|^2 + (\tilde{a})^2 S^* + (a\tilde{a}^* + a\tilde{a})S + a\rho^* \\ &\quad + (\tilde{a} + 1)\rho . \end{aligned} \tag{3.21}$$

This represents three parametric constraints

$$|a|^2 + (\tilde{a})^2 = 1 , \tag{3.22a}$$

$$a(\tilde{a}^* + \tilde{a}) = 0 , \tag{3.22b}$$

$$a\rho^* + (\tilde{a} + 1)\rho = 0 . \tag{3.22c}$$

Eq. (3.22c) expresses a in terms of ρ and $\tilde{a}$. Eq. (3.22b) implies that $\tilde{a}$ is pure imaginary. Eq. (3.22a) is redundant. Eq. (3.18a), simplified in accordance with (3.22), becomes

$$S' = -\frac{\rho}{\rho^*}(1 + i\beta)S + i\beta S^* + \rho , \tag{3.23}$$

where the real parameter $\beta \equiv -i\tilde{a}$. We defer discussing how to estimate β until the end of this analysis.

Consider now the effect of two $K\bar{K}$ reflections, one at time zero and the other at time T, on the kink and antikink shape modes, when the initial state has no shape oscillation at all. Since the initial amplitude S is zero, the amplitude after the first impact, according to (3.23), is ρ. The amplitude after the second impact, according to (3.23) [modified according to (3.18b)], is then

$$S'' = -\frac{\rho}{\rho^*}(1 + i\beta) + i\beta\rho^* e^{-2i\omega_s T} + \rho\, e^{-i\omega_s T} . \tag{3.24}$$

Thus the energy in shape oscillation after two impacts is

$$\begin{aligned} 4|S''|^2\omega_s^2 &= 16\omega_s^2|\rho|^2 \cos^2\frac{\omega_s T}{2} \\ &\quad \times \left|1 - 2\beta\, e^{-i\omega_s T/2} \sin\frac{\omega_s T}{2}\right|^2 . \end{aligned} \tag{3.25}$$

We have used eq. (3.20) in deriving (3.25).

Eq. (3.25) implies that no energy is in the shape oscillations – i.e., the kink speed is unchanged after two collisions – for $\omega_s T = (2n + 1)\pi$, which is precisely the condition (2.6) that characterizes the window centers (recall $\delta = 3.3 \approx \pi$).

To obtain the angular width, θ, of the windows, one then solves the equation obtained from (3.25) by replacing ωT in the right-hand side by $(2n + 1)\rho \pm \theta/2$, and replacing the left-hand side by $Mv^2 \approx Mv_c^2 = 4\omega_c^2|\rho|^2$; the result is

$$1 = 4\sin^2\frac{\theta}{4}\left|1 + 2i\beta\, e^{\pm i\theta/4}\cos\frac{\theta}{4}\right|^2 . \tag{3.26}$$

Expanding the right-hand side of (3.26) in powers of θ and retaining only the leading order, one obtains

$$\theta \approx 2/\sqrt{1+4\beta^2}. \tag{3.27}$$

The desired estimate, $\theta \leqslant 2$, follows immediately, and from the empirical fact that θ appears to saturate the bound, one concludes that $\beta \ll 1$. With $\beta = 0$, it is apparent that (3.26) has $\theta = 2\pi/3 \approx 2.1$ as its only solution between zero and π. Thus the theory accounts for the observed result that there is only one smooth "two-bounce" window for each integer n.

Finally, we refer the reader to fig. 8 for a more direct check of the crucial assumption of nearly conservative transfer of energy between the shape and translational modes. The horizontal axis in this figure represents incoming kink speed; the vertical axis represents the ratio of outgoing to incoming speeds, for those initial speeds that do not lead to the $K\bar{K}$ capture. The approximation of conservative transfer relied on in this subsection implies that each peak to the left of $v = v_c$ has a maximum value close to unity, as can be seen to be the case.

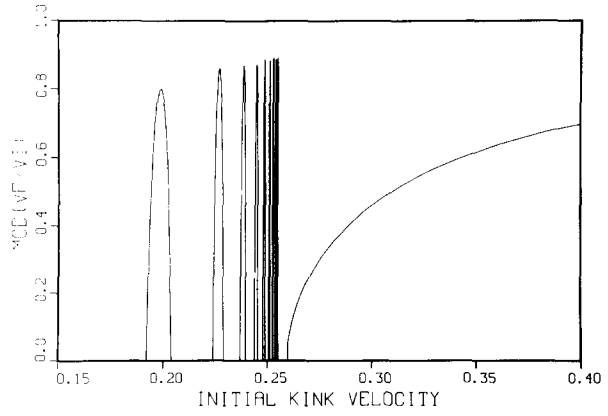

Fig. 8. The ratio of the (time-averaged – see section 4) kink speed after a $K\bar{K}$ collision to the initial speed, as a function of the initial velocity. Note the relatively elastic nature of the reflections below v_c.

4. Fine structure in $\phi(0,t)$ and v_f

4.1. *Background*

In the preceding sections we have focussed primarily on the resonance windows and in particular on the critical role of the shape mode oscillations in determining these resonances. With few exceptions, we have neglected the role of the "radiation" emitted by the collisions, and we have treated the final kink velocity, v_f, as if it were a constant in time. In this section, we will correct these omissions by discussing in detail the role of radiation in $K\bar{K}$ collisions and by describing some interesting "fine structure" in the time dependence of the final velocity. We shall see that these effects are related.

With regard to the resonance phenomenon, radiation plays the important role of an energy "sink", essentially removing energy from the $K\bar{K}$ translation and shape modes in a manner that precludes the retransfer to the bound $K\bar{K}$ pair. As we have argued previously, this provides a natural limit to the total number of observable windows of a given bounce number. In fig. 9 we show how, at a time $T = 95$ units after the first $K\bar{K}$ collision, the initial $K\bar{K}$ kinetic energy is distributed among the $K\bar{K}$ kinetic energy, shape mode energy, and radiation.* We see that, except for the highest velocities, the shape mode does absorb most of the lost kinetic energy. Nonetheless, the radiation modes clearly are excited in the collisions.

Before discussing this radiation in detail, let us first describe the (related) "fine structure" in the final kink velocity, v_f. This "fine structure" is

* Since the different modes among which the energy is distributed represent *linear* modes around a single kink, there is clearly some ambiguity in extracting the energy sharing from the numerical solution to the full *nonlinear* equation. As we are only interested in the rough partitioning of energy, it is sufficient for us to adopt the following prescription: (1) the kinetic energy of the K and $\bar{K}$ is Mv_f^2, where v_f is the average final velocity; (2) the energy in the region beyond 5 units from the kink is called radiation; and (3) the remaining energy is taken to be in the shape mode. This slightly overestimates the energy in the shape mode because it includes a small amount of decay radiation in the immediate vicinity of the wobbling kinks.

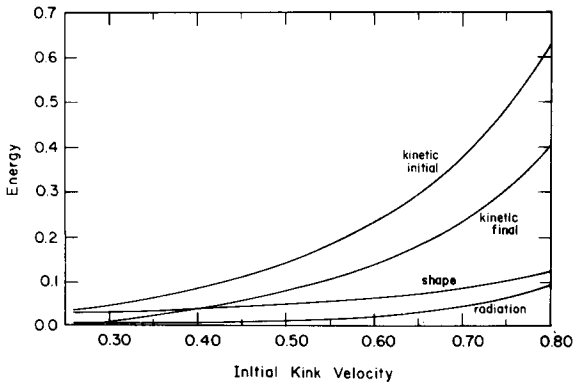

Fig. 9. The partitioning of the initial $K\bar{K}$ kinetic energy into final kinetic energy, shape mode energy, and radiation energy, plotted as a function of the initial $K\bar{K}$ speed for $v > v_c$.

shown in fig. 10, which plots $v_f(t)$ versus t for six values of the initial velocity greater than v_c. Note that v_f does not quickly approach an asymptotic value but instead oscillates rapidly about a mean. These oscillations, which range from roughly 15% of the mean for the lowest initial velocity shown to roughly 5% for the highest, are the "fine structure". In our previous discussion and figures, where a single asymptotic kink velocity was mentioned and plotted, we used the mean value of v_f as determined by averaging over a time $T_{av} = 20.0$, which was chosen to be longer than any oscillation period observed in the numerical data. Although one might initially question this averaging when the velocity undergoes such sizable and rapid oscillations, we feel that the explanation presented in this section answers any questions on this point. A relevant remark on this matter is that the "fine structure" is not limited to the behavior of $v_f(t)$ but is also observed in $\phi(x = 0, t)$. Fig. 11 shows $\phi(x = 0, t)$ versus t for six values of initial velocity. The rapid small oscillations are similar (but not

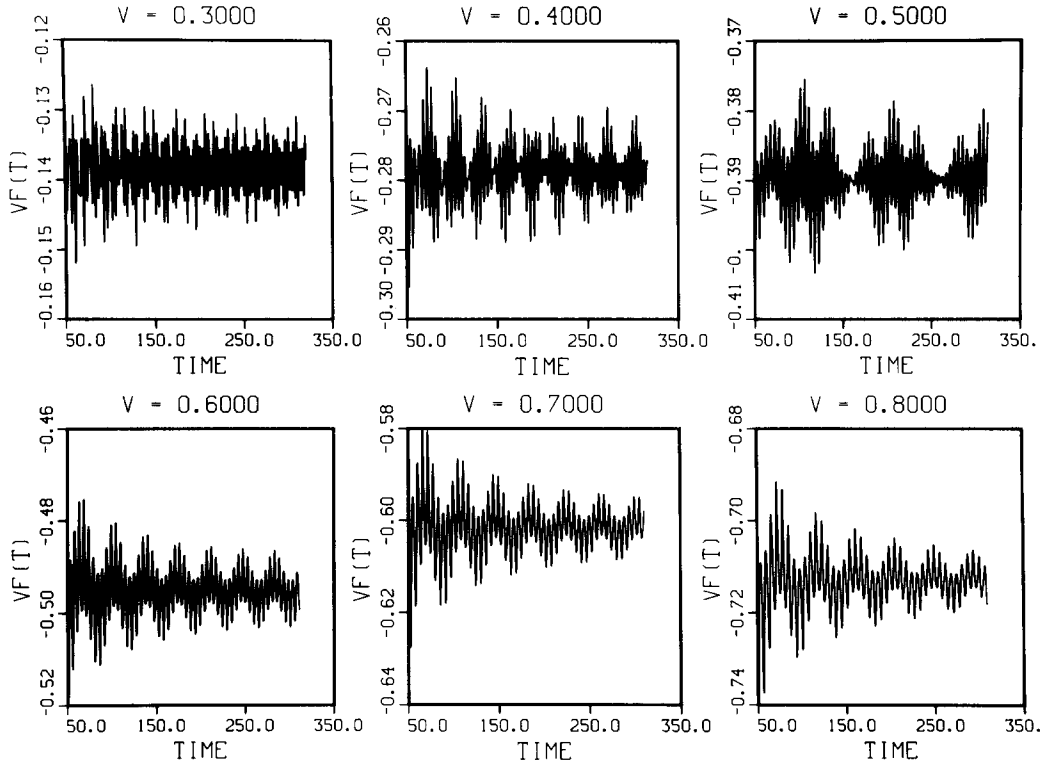

Fig. 10. The kink velocity after a $K\bar{K}$ collision $[v_f(t)]$ as a function of time for initial kink velocities of 0.3, 0.4, 0.5, 0.6, 0.7, and 0.8, respectively. The collisions occurred at times 20.7, 16.3, 13.6, 11.7, 10.3, and 9.2.

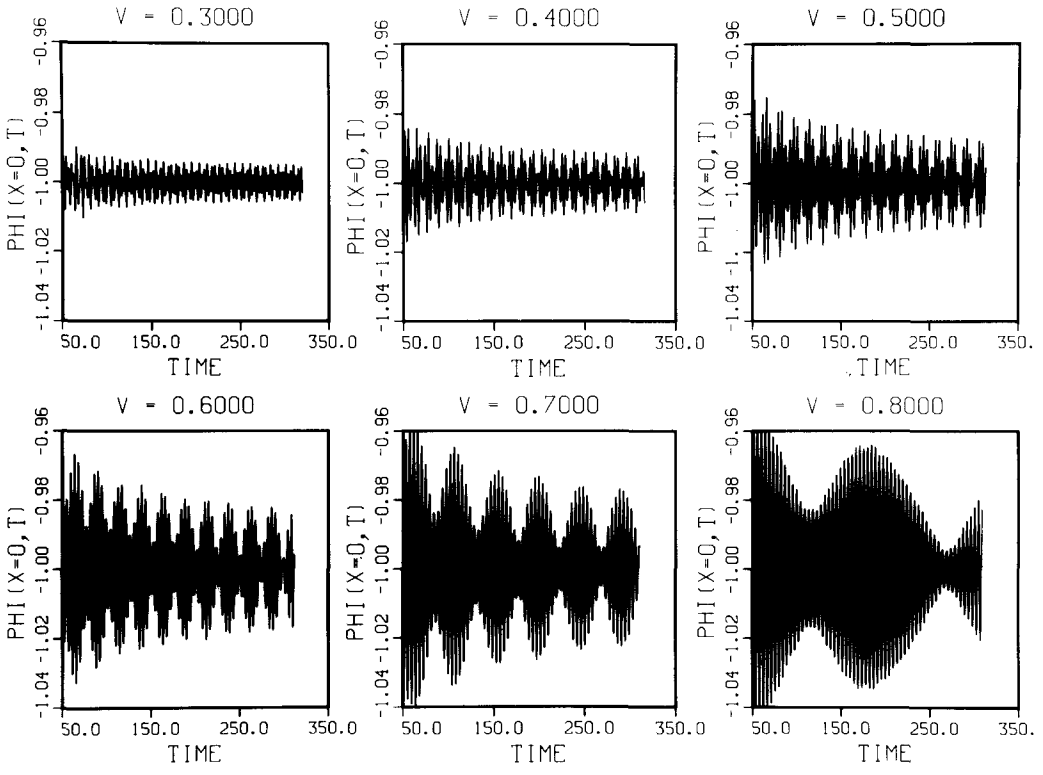

Fig. 11. $\phi(x=0,t)$ versus t after a K$\bar{\text{K}}$ collision for initial kink speeds of 0.3, 0.4, 0.5, 0.6, 0.7, and 0.8, respectively.

identical to) those seen in $v_f(t)$, as illustrated in fig. 10. To simplify the interpretation of figs. 10 and 11, we have calculated the power spectra of the fast Fourier transforms of these data in figs. 12 and 14, respectively. Fig. 13 shows parts of fig. 12 but with an expanded horizontal scale. Note that the horizontal scale represents periods of oscillation rather than angular frequency, which would be 2π/(period). From these power spectra it is clear that the fluctuations in figs. 10 and 11 are dominated by a few discrete frequency components. In the remainder of this section we shall argue that these frequencies can be understood qualitatively in terms of radiation and its coupling to other modes.

Both from the energy partition graph of fig. 9 and from the success of our arguments in the preceding sections, we expect that the radiation amplitudes are small. Thus, at least in the regions away from the K and $\bar{\text{K}}$, we expect that to good approximation they can be treated by simple linear superposition. Near the kinks – and thus for quantities like $v_f(t)$ which are related to the kink motion – the effects of radiation may be complicated by small but nonzero coupling to the kink shape oscillation. These expectations are consistent with figs. 12–14, which show that $\phi(x=0,t)$ contains just two dominant frequencies for all incoming kink speeds, whereas the spectra of $v_f(t)$ show considerably more structure.

4.2. *Quantitative results and fine structures in* $\phi(x=0,t)$

To clarify the role of the radiation in both these structures, it is important to distinguish two distinct components. The first component – which we shall henceforth call "prompt" radiation – is gener-

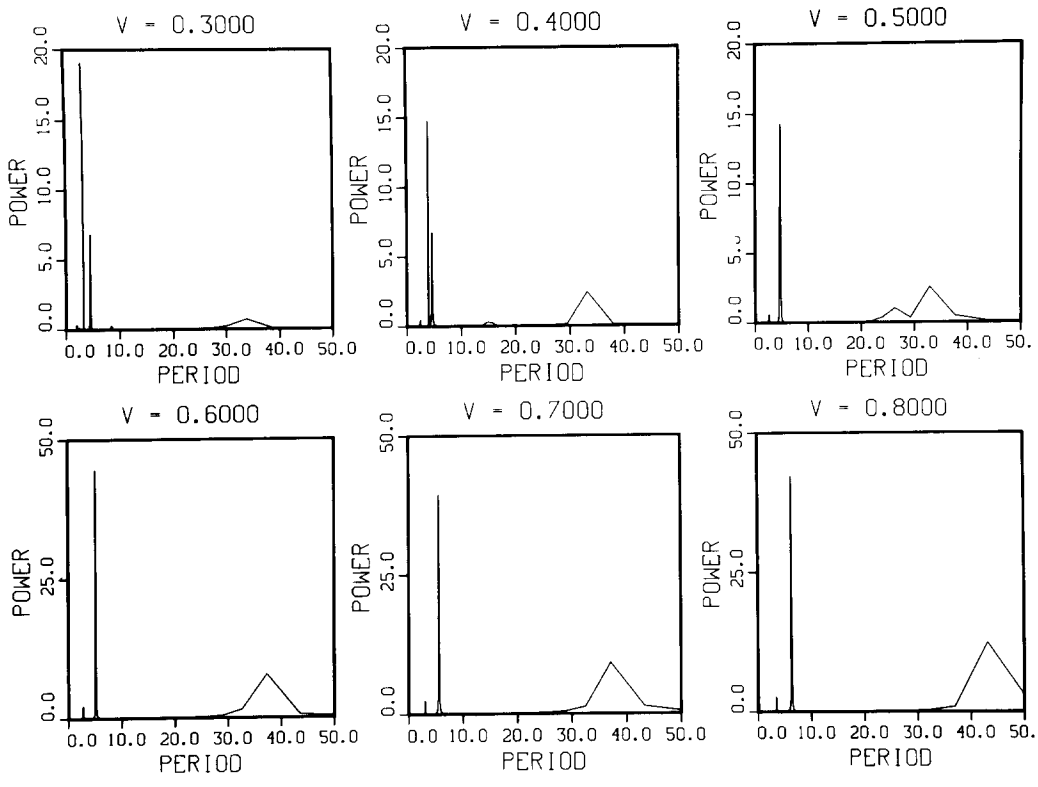

Fig. 12. The power spectrum of $v_f(t)$ versus oscillation period ($= 2\pi$/angular frequency). This figure was generated by a fast Fourier transform of the numerical data in fig. 10. The vertical scale is multiplied by 10^6.

ated at the "instants" of K$\bar{\text{K}}$ impact. The second component – which we shall call "decay radiation" – arises from the decay of the shape oscillations of the kink and antikink. Specifically, since a "wobbling", translating kink is *not* an exact solution to the full *nonlinear* equations*, the shape mode will decay in second order in the expansion of eq. (1.4) around the K or $\bar{\text{K}}$.

To model the effects of the prompt radiation (away from the kink and antikink centers), we consider the solution P to the linearized – that is, small amplitude – version of eq. (1.4) with a δ function source,

$$\partial_t^2 P - \partial_x^2 P + 2P = c\delta(x)\delta(t)\,, \tag{4.1}$$

with $P(x, t) = 0$ for $t < 0$. We shall not attempt to determine the proportionality constant, c. Eq. (4.1) represents the production of freely propagating relativistic waves of mass $\sqrt{2}$ (the continuum threshold for small oscillations about K or $\bar{\text{K}}$) by an instantaneous source. The instantaneous source idealizes the K$\bar{\text{K}}$ impact; t here is time from impact.

The solution to (4.1) is

$$P(x, t) = c\int \mathrm{d}\omega\, \mathrm{d}k \{\mathrm{e}^{\mathrm{i}(\omega t + kx)}/(\omega^2 - k^2 - 2)\}$$
$$= c\theta(t - |x|)J_0(\sqrt{2(t^2 - x^2)})\,, \tag{4.2}$$

* Note that a purely translating kink (with the appropriate Lorentz contraction) *is* an exact solution of the full nonlinear equation. This emphasizes the distinction between a "true" collective coordinate (corresponding to an invariance of the solution) and in "approximate" collective coordinate, as discussed in appendix B.

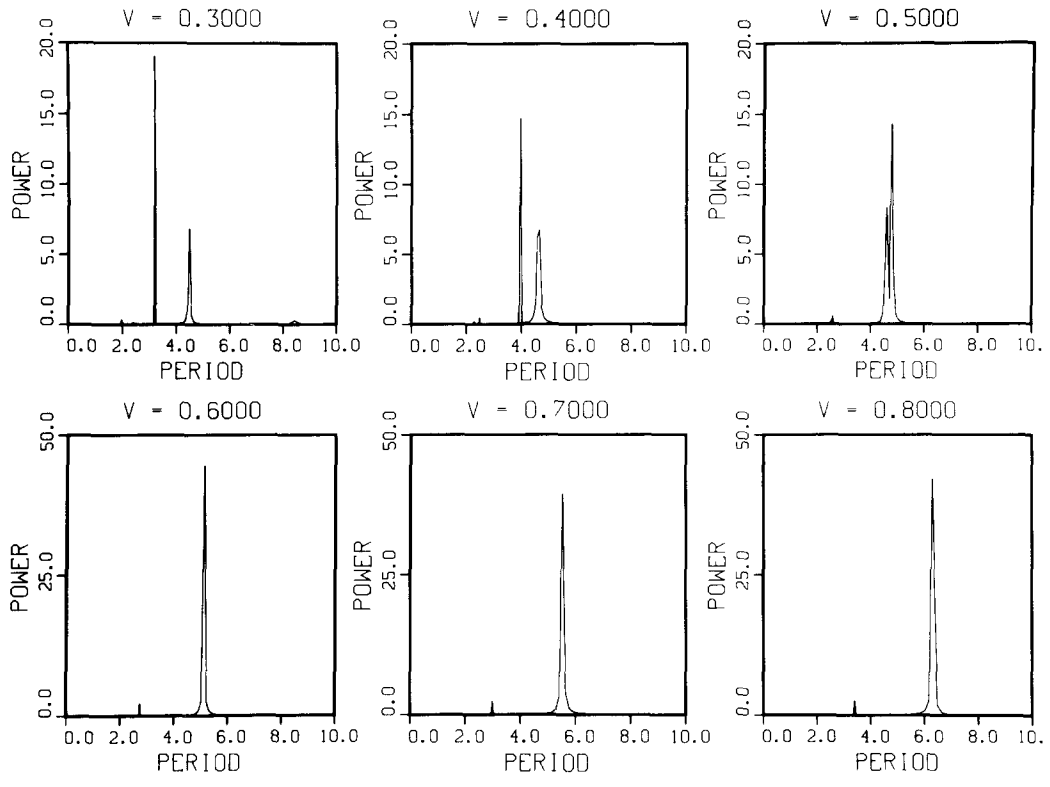

Fig. 13. The same as fig. 12 but with an expanded horizontal scale.

where the causal boundary condition on P has determined how one integrates around the poles. J_0 is the usual Bessel function, and θ is the Heaviside step function. For $\sqrt{2(t^2-x^2)} \gtrsim 1$, we may use an asymptotic form for J_0, replacing (4.2) by

$$P(x,t) \approx c\theta(t-|x|)\frac{\cos\sqrt{2(t^2-x^2)}}{(t^2-x^2)^{1/4}}. \tag{4.3}$$

This result enables us to understand half of the dominant structure in fig. 14. According to (4.3), $P(x=0)$ is approximately proportional to $t^{-1/2}\cos t\sqrt{2}$ for $t \gg 0$. From this we conclude that the Fourier spectra in fig. 14 should all display a peak at the fixed period $2\pi/\sqrt{2} \approx 4.4$, which is indeed the case. We shall indicate some signatures of the $1/\sqrt{t}$ envelope at the end of this section.

For future reference, we note here that in the Lorentz frame of and near a kink moving out from the collision at velocity $v_0 > 0$ – that is, for $|x - v_0 t| \ll tv_0$* – the radiation from the solution in (4.3) has the approximate form

$$P(x,t) \approx c(1-v_0^2)^{-1/4}t^{-1/2} \times \cos\left(\frac{t\sqrt{2}}{\sqrt{1-v_0^2}} - \frac{xv_0\sqrt{2}}{\sqrt{1-v_0^2}}\right). \tag{4.4}$$

Apart from the $1/\sqrt{t}$ envelope, this is simply a plane wave of frequency $\sqrt{2}/\sqrt{1-v_0^2}$, and dispersion relation $\omega^2 - k^2 = 2$ [as required by (4.1)]. The presence of the kink locally deforms such plane waves (see, for example, eq. (2.9) of [8]), but

* Here and elsewhere in this section we ignore constants in the equation ($x_0 = v_0 t + c_0$) describing the outgoing kink average position. The value of c_0 is important mainly for the phases of the oscillations, whereas our principal concern here is with the frequencies.

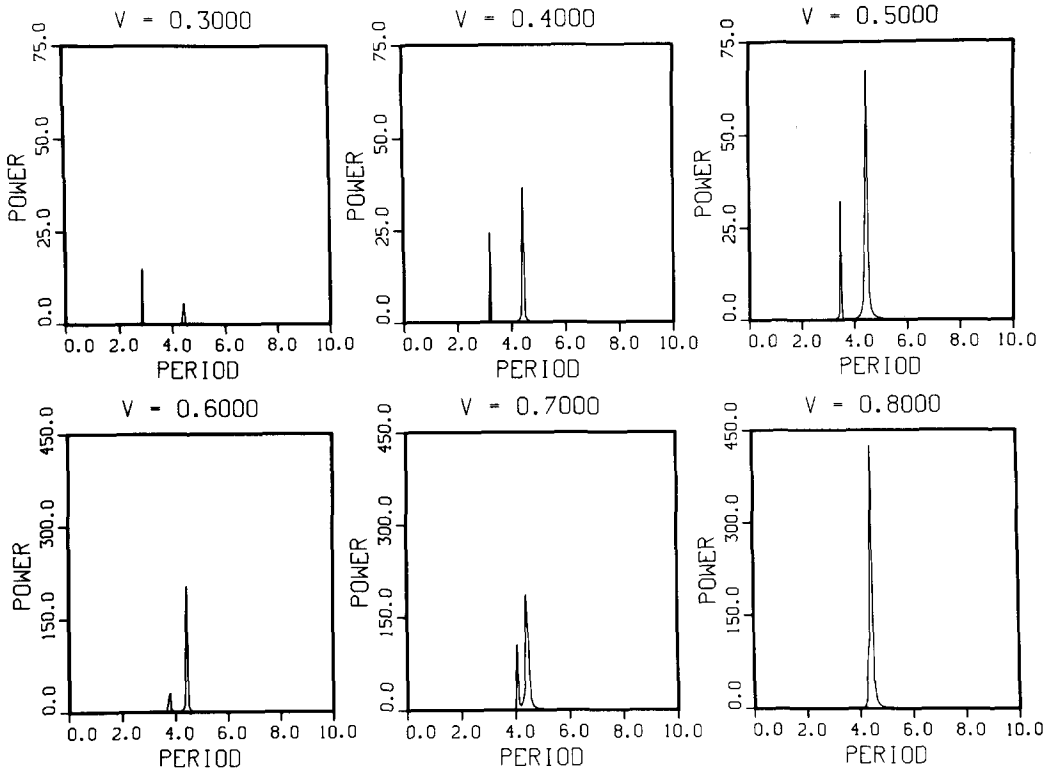

Fig. 14. The power spectrum of $\phi(x=0,t)$ versus oscillation period ($=2\pi$/angular frequency). This figure was generated by a fast Fourier transform of the numerical data in fig. 11.

we shall not need to take this deformation into account below.

The field perturbation due to the "decay" radiation from the kink (antikink) shape mode is presumably dominated (in the K($\bar{K}$) rest frame) by the second order term in an expansion about $\phi_{K(\bar{K})}$, whose first order term is the shape oscillation itself. The truncation of eq. (1.4) that describes how a second-order disturbance (ϕ_2) is determined by a first order one (ϕ_1) is

$$(\partial_t^2 - \partial_x^2 + 3\phi_{K(\bar{K})}^2 - 1)\phi_2 = -3\phi_{K(\bar{K})}\phi_1^2 . \qquad (4.5)$$

It follows from (4.5) that if ϕ_1 is shape oscillation at $\omega = \omega_s = \sqrt{3}/\sqrt{2}$, then ϕ_2 a priori contains components of angular frequencies zero and $2\omega_s = \sqrt{6}$. However, since the continuum for linear-order propagation is $\omega = \sqrt{2}$, the response at zero frequency does not extend to large distances, and one is left with only $\omega = \sqrt{6}$ available for long-range effects.

Thus we model radiation due to kink (antikink) shape mode decay in the kink (antikink) rest frame, by a field perturbation proportional (far from the source) to $\cos(\sqrt{6}t - 2|x|)$ (up to phase), cut off at $|x| \gtrsim t\sqrt{2/3}$. This represents a plane wave of frequency $\sqrt{6}$, propagating (with dispersion law $\omega^2 - k^2 = 2$) away from the kink (antikink)* source at the origin of the coordinate system. The

* One also expects a slow exponential damping factor. However, the decay time appears to be too long for such a modulation to be conspicuous in our data, and so we choose not to include it in our Ansatz.

wavefront moving outward at the group speed $\sqrt{2/3}$ is required since the shape mode begins "broadcasting" only at $t \approx 0$ when it is formed in the $K\bar{K}$ collision. As in the case of prompt radiation, we shall not need detailed information about the way that the kink (antikink) deforms the waveform of the radiation emitted in the course of antikink (kink) shape-mode decay.

In the "laboratory frame" – that is, the frame of our computer simulation – the radiation emitted by the shape mode of the kink (antikink) that leaves the collision region at (average) velocity $\pm v_0$, as seen to the left (right) of the kink (antikink), is described by a field perturbation proportional to

$$\cos\left(t\left(\frac{\sqrt{6}-2v_0}{\sqrt{1-v_0^2}}\right) \pm x\left(\frac{2-\sqrt{6}v_0}{\sqrt{1-v_0^2}}\right)\right), \tag{4.6}$$

up to phase. The fronts of these wavetrains move at speed

$$(\sqrt{2/3} - v_0)/(1 - v_0\sqrt{2/3}). \tag{4.7}$$

These are consequences of Lorentz invariance.

These results enable us to understand the remaining half of the dominant structure in fig. 14. It follows from (4.6) that decay radiation from both kink and antikink contributes signals of the same angular frequency $(\sqrt{6}-2v_0)/(1-v_0^2)^{1/2}$ to $\phi(x=0)$. The third column of table II displays the period associated with this angular frequency for each incoming speed represented in the sequence of pictures in fig. 14. The average outgoing speeds v_0 in the second column are taken from the pictures in fig. 10. These periods compare well with the periods corresponding to the left of the two peaks in the spectra of fig. 14. For an incoming speed $v = 0.8$ this peak is too close to that corresponding to prompt radiation $(2\pi/\sqrt{2})$ to be distinguished clearly in the Fourier spectrum. We have, accordingly, listed in the last column of table II the period of beating between these two theoretical frequencies, for direct comparison with the time-domain data in fig. 10.

Table II
A tabulation of the expected frequencies in $\phi(x=0,t)$ for different initial velocities (v) and observed averaged final velocity (v_0). The third column represents the period of the shape mode "decay radiation", whereas that in the fourth column is the period corresponding to the beating of this frequency with the "prompt" radiation

v	v_0	$2\pi\sqrt{1-v_0^2}/(\sqrt{6}-2v_0) \equiv 2\pi\Omega^{-1}$	$2\pi(\Omega-\sqrt{2})^{-1}$
0.3	0.14	2.9	8.1
0.4	0.28	3.2	11.3
0.5	0.39	3.4	15.8
0.6	0.50	3.7	23.6
0.7	0.60	4.0	42.5
0.8	0.71	4.3	136.6

Note that according to (4.7), the wavefronts of decay radiation cannot reach the origin for $v_0 > \sqrt{2/3} \approx 0.82$, and so decay radiation can make no contribution to $\phi(x=0)$ in this case. None of the speeds in the second column of table II exceed this threshold. Note, however, that the critical outgoing speed beyond which the wavefront of kink (antikink) decay radiation cannot reach the *receding antikink* (*kink*) is $\frac{1}{2}(\sqrt{6}-\sqrt{2}) \approx 0.52$, which is the physical solution of the equation

$$v_0 = (\sqrt{2/3} - v_0)/(1 - v_0\sqrt{2/3}). \tag{4.8}$$

Beyond this threshold, decay radiation should make no contribution to the fine structure in the time-dependence of kink or antikink speed. Two outgoing speeds in table II do pass this point, and a third comes close. There are clear signatures for this in the fine structure in $v_f(t)$, as we shall point out shortly.

4.3. *Fine structure in* $v_f(t)$

The computer program that generated the velocity data shown in fig. 10 defines "kink position" as the largest positive value of x at which the field ϕ crosses zero. Writing

$$\phi = \tanh\left(\frac{x}{\sqrt{2}}\right) + \delta\phi \tag{4.9}$$

for the field configuration near the kink in its (average) rest frame, we see that the zero crossing is

$$x_0 \approx -\sqrt{2}\delta\phi(x,t)|_{x=0} \tag{4.10}$$

to first order in $\delta\phi$. An observer in the laboratory frame sees this as*

$$x_0 \approx v_0 t - \sqrt{2}\sqrt{1-v_0^2}\,\delta\phi(x, t\sqrt{1-v_0^2})|_{x=0}\,. \tag{4.11}$$

The rest frame of the kink is useful for our purposes because, in view of the time-independence of the linear-order equation (2.3), it permits a convenient frequency analysis of perturbations like $\delta\phi$. In the kink rest frame, the field configuration (4.4) of nearby prompt radiation becomes

$$(\text{constant}) \times (t + v_0 x)^{-1/2} \cos t\sqrt{2}\,, \tag{4.12}$$

and the field configuration (4.6) of nearby radiation from antikink shape-mode decay becomes

$$(\text{constant}) \times \cos\{(1-v_0^2)^{-1}[t(\sqrt{6}(1+v_0^2) - 4v_0) - x(2(1+v_0^2) - 2\sqrt{6}v_0)]\}\,. \tag{4.13}$$

These are consequences of the Lorentz invariance of eq. (1.4).

In the present instance, $\delta\phi$ is a sum of four terms, representing four distinct effects: (1) a shape-mode solution, s, to the linearized equation (2.4); (2) a continuum eigenmode, d, of (2.4) approaching the decay radiation form (4.13) at large ($\gtrsim 1/\sqrt{2}$) distances from the kink center; (3) another continuum eigenmode, p, of (2.4) approaching the prompt radiation form (4.12)†; and (4) a remainder, r, representing the (presumably) small effects of the nonlinear coupling of d, p, and s.

Recalling the discussion of shape mode decay in the preceding subsection, we suppose that the dominant contribution of r comes from the second order term in an expansion of ϕ whose first order term is $d + p + s$. Thus, a priori, according to (4.11), we expect the dominant terms in $\dot{x}_0$ to have angular frequencies

$$\Omega_d \equiv [\sqrt{6}(1+v_0^2) - 4V](1-v_0^2)^{-1/2}\,,$$
$$\Omega_p \equiv \sqrt{2}(1-v_0^2)^{1/2}, \quad \Omega_s \equiv \sqrt{3/2}(1-v_0^2)^{1/2} \tag{4.14}$$

(i.e., $\sqrt{1-v_0^2}$ times the frequencies of d, p, and s, respectively), and also all sums and differences of the frequencies in (4.14), taken two at a time.

However, not all the frequencies that are a priori available will correspond to significant effects in $\delta\phi$. Components with frequency Ω_s or $\Omega_s \pm \Omega_s$ can play no role. They arise from the coupling of the spatially antisymmetric shape mode to the spatially antisymmetric kink; and since the field equation (1.4) is invariant under $x \leftrightarrow -x$, this can only produce spatially antisymmetric contributions to $\delta\phi$. In particular, such terms in $\delta\phi$ must vanish identically at $x = 0$.

Components with frequencies $\Omega_d \pm \Omega_d$, $\Omega_p \pm \Omega_p$, and $\Omega_d \pm \Omega_p$ are also expected to be relatively unimportant. They correspond to terms in $\delta\phi$ that are $\mathcal{O}(d^2)$, $\mathcal{O}(p^2)$, and $\mathcal{O}(pd)$, respectively. In view of the small amount of energy in radiation (as compared with shape modes) such contributions should be insignificant next to terms in $\delta\phi$ that involve only one power of d and/or p.

Thus we conclude from our radiation model that components with the following angular frequencies should dominate the Fourier spectra of $\dot{x}_0$, shown in figs. 12 and 13:

$$\Omega_d, \quad \Omega_p, \quad \Omega_d \pm \Omega_s, \quad \Omega_p \pm \Omega_s\,. \tag{4.15}$$

These correspond to terms in $\delta\phi$ that are $\mathcal{O}(d)$, $\mathcal{O}(p)$, $\mathcal{O}(ds)$, and $\mathcal{O}(ps)$, respectively.

* Here and elsewhere in this section we ignore constants in the equation ($x_0 = v_0 t + c_0$) describing the outgoing kink average position. The value of c_0 is important mainly for the phases of the oscillations, whereas our principal concern here is with the frequencies.

† We shall regard the envelope $(t + v_0 x)^{-1/2}$ as a slow adiabatic effect that can be treated as a constant when analyzing the rapid oscillations of the kink.

The periods associated with the angular frequencies listed in (4.15) are catalogued in table III, for all the values of v corresponding to the data shown in figs. 12 and 13. These periods compare well with the periods corresponding to the peaks in the spectra of figs. 12 and 13.

For $v = 0.5$ and 0.6 the periods involving Ω_p are too close to those involving Ω_d to be distinguished clearly in the Fourier spectra. As in table II, we have listed in the last column of table III the period of beating between these two sets of theoretical frequencies. The patterns visible in fig. 10 are consistent with the figures listed in this column.

Note that for $v = 0.7$ and 0.8, table III contains no entries in columns listing periods involving Ω_d. As indicated at the end of the preceding subsection, for these speeds antikink decay radiation cannot contribute to kink velocity because the antikink decay radiation wavefront travels more slowly than the outgoing kink. In particular there should be no beats visible in the pictures corresponding to these speeds in fig. 10, and this is indeed the case.

We are now in a position to comment on experimental signatures of the $1/\sqrt{t}$ modulation in p. It follows from the foregoing discussion that for $v = 0.7$ and 0.8 all the dominant contributions to $\dot{x}_0$ come from contributions to $\delta\phi$ that are of first order in p. Thus we expect the oscillations in the last two pictures in fig. 10 to be under an envelope approximately proportional to $1/\sqrt{t}$, which is indeed so.

The $1/\sqrt{t}$ envelope is also apparent in fig. 15,

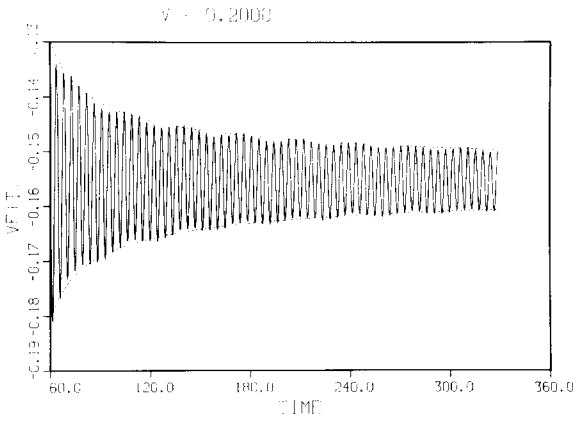

Fig. 15. The kink velocity after $K\bar{K}$ collision as a function of time for an incoming speed of $v = 0.2$ near the center of the widest two-bounce window (solid curve). The dashed curve is a fit of the envelope to (constant) $\times (t - t_{\text{last collision}})^{-1/2}$. The second impact occurred at time $T = 47$.

which shows oscillations in outgoing kink speed when the incoming speed is equal to 0.2, which is the midpoint of the largest two-bounce window. To understand this figure, recall from section 3 that for such a value of v, the energy in shape oscillation – and therefore also in "decay" radiation – is minimal. Therefore, of the six frequencies listed in (4.15), only that corresponding to the "prompt" radiation – Ω_p is expected to appear in the vibrations shown in fig. 15. Since the term is $\delta\phi$ with frequency Ω_p is p itself, the $1/\sqrt{t}$ modulation must appear. Note that this argument is somewhat oversimplified, since for $v = 0.2$ – as for all incoming speeds below v_c for which the K

Table III
A tabulation of the different periods expected to occur in $v_K(t)$ for different initial velocities (v). The average final velocity is v_0

v	v_0	$\frac{2\pi}{\Omega_d+\Omega_s}$	$\frac{2\pi}{\Omega_p+\Omega_s}$	$\frac{2\pi}{\Omega_d}$	$\frac{2\pi}{\Omega_p}$	$\frac{2\pi}{\Omega_d-\Omega_s}$	$\frac{2\pi}{\Omega_p-\Omega_s}$	$\frac{2\pi}{\Omega_p-\Omega_d}$
0.3	0.14	2.0	2.4	3.2	4.5	8.4	33.4	11.2
0.4	0.28	2.3	2.5	4.0	4.6	15.4	34.5	27.7
0.5	0.39	2.5	2.6	4.6	4.8	25.9	36.1	91.1
0.6	0.50	2.7	2.7	5.1	5.1	37.6	38.1	3141.6
0.7	0.60	—	3.0	—	5.6	—	41.3	—
0.8	0.71	—	3.4	—	6.3	—	47.2	—

and $\bar{K}$ escape to infinity – there are *two* $K\bar{K}$ "impacts" and hence *two* sources (differing in the time of their emission) of "prompt" radiation. Nonetheless, both of these should, for t large compared to both collision times, fall off like $1/\sqrt{t}$ and hence the envelope seen in fig. 15 is still anticipated by our arguments.

5. Concluding remarks

When the details are stripped away, the central idea underlying our mechanism for the structure in kink/antikink collisions is a resonant energy exchange between the translational – "center of mass" – motion of the two kinks and an isolated (in frequency) shape mode oscillation internal to each kink. Clearly this mechanism is not restricted to the ϕ^4 theory, and thus from a mathematical standpoint, the phenomenon of parametric windows of escape that alternate with regions of capture should not be regarded as exceptional. Indeed, this phenomenon has been observed previously [38] in what initially seems an entirely different context: namely, in time-dependent Hartree–Fock (TDHF) calculations of nuclear collisions in a (quasi)-one-dimensional geometry. From a mathematical perspective, the TDHF-equations can be viewed as a set of coupled, *non*integrable nonlinear Schrödinger equations [2, 38], and it is thus not terribly surprising that they could illustrate the resonance phenomena. Interestingly, in TDHF the individual "solitary waves" – which are just the individual nuclei – *do* have (at least) two isolated, internal shape mode oscillations [38]. As a function of relative velocity, the collisions of these "nuclei" show two clear escape ("scattering") windows below the first capture ("fusion") threshold. It is possible that more extensive numerical study would reveal further windows, but it is also possible that the existence of two competing internal modes destroys the fine details of the resonance mechanism.

Very recently, a numerical study [39] of a parametrically modified sine-Gordon-like model [10], in which the familiar potential $V(u) = (1 - \cos u)$ is replaced by

$$V(u) = (1 - r)^2 \frac{(1 - \cos u)}{(1 + r^2 + 2r \cos u)}, \tag{5.1}$$

has revealed similar window structure. For values of r such that there exists one isolated internal shape mode ($0 > r \gtrsim -0.2$), the two-bounce window theory provides excellent agreement with the data. For values of r such that there are many internal shape modes, some windows remain but the fine detail of the two-bounce predictions is washed out. This is qualitatively consistent with the TDHF results [38].

A crucial question requiring further investigation is whether the requirement of an internal oscillation, localized about the solitary wave, is absolutely essential to the resonance phenomenon. Intuitively, one might initially expect that a "wave packet" of continuum modes, centered about some specific frequency, ω_{peak}, could be set up by the initial collision and later resonantly "return" its energy to the translation mode. For kink interactions in more general models – in particular, for collisions in which the kink and antikink never clearly separate as they do between the two bounces in ϕ^4 – we certainly can not exclude this possibility. Nonetheless, the observations that (1) continuum modes disperse, rather than remaining localized with the kinks and (2) the existence of (a continuum of) other modes near ω_{peak} should lead to a "washing out" of detailed resonance structure suggest that this possibility is unlikely. Interestingly, results [39] on the model described by eq. (5.1) suggest that, for those values of r for which there are no kink shape modes ($r > 0$), there is also no resonance structure in $K\bar{K}$ collisions. To answer this question properly will require making a rigorous distinction, at least in perturbation theory, between the localized and continuum modes around a single kink [41].

Let us now turn to the potential physical implications of our analysis. Quite generally, the phenomenon of resonant capture/escape alternation should be observable in interactions of many types

of extended objects (not necessarily restricted to one dimension) that support isolated modes of internal vibration that do not damp out too rapidly*. At a more specific level, one can look for direct applications of the one dimensional ϕ^4 theory in quasi-one-dimensional solid state systems [6–20]. The possibility that these resonance effects might arise in the equilibrium thermodynamics of these systems [11, 12, 16, 17] as, say, clear modifications of *independent* kink motion, seems remote, for the velocity range spanned by the resonance is very small, and the bulk behavior of these materials involves many kinks and antikinks, with the shape modes of each excited by differing amounts. However, the more general effect that ϕ^4 kinks capture at low relative velocity and reflect at high may be of consequence to some thermodynamic quantities.

In the time-dependent dynamics [7, 8, 10–17] of these systems, however, the effects of this resonance structure may prove more interesting. It may effect, for example, cluster formation [13, 14] and consequently the behavior of dynamic correlation functions. Further, if one considers the mechanism underlying the resonances – that is, the exchange of energy between translation and shape oscillation – a number of questions for further study arise. If, for example, kink–antikink bound states are responsible for characteristic enhancements away from zero frequency in certain dynamic correlation functions, it is possible that this exchange could lead to broadening of these enhancements because it makes the $K\bar{K}$ binding energy – and therefore the bound orbital period – less well-defined. Of course, for closely-bound $\bar{K}K$ pairs, it becomes hard to make sense out of the notion of well-defined shape modes for the individual kinks. Indeed, this is precisely the reason given in section 2 for the absence of the windows corresponding to the lowest integers ($n = 0, 1, 2$). Nonetheless, this application seems to merit further study.

Finally, an interesting potential application of the shape mode-translation coupling has been suggested [19, 42] in the context of a phenomenological ϕ^4 model of polyacetylene [$(CH)_x$] [18, 19]. The hope is to excite the shape modes of charged kinks in $(CH)_x$ by illumination with light of the appropriate frequency. If the shape mode-translation coupling is strong enough, this could result in an increase in the effective soliton temperature sufficient to decrease perceptibly the electrical conductivity. In this context, it is important to note that this shape mode is apparently not an artifact of the ϕ^4 model, as calculations [43] in more *microscopic* models of $(CH)_x$ reveal the same sort of shape mode.

* Even in macroscopic bodies one can imagine such effects. The problem is to identify objects with a small number of isolated internal modes which are not strongly damped. For most potential examples – such as close encounters of stars whose seismic vibrations can be excited by tidal forces – there are either too many modes or too much damping for the resonance phenomenon to be expected.

Acknowledgements

Over the (long) course of this work we have benefited greatly from extensive advice and suggestions from many colleagues, and it is impossible to mention all these debts properly. Special thanks are due to J.R. Schrieffer and D. McLaughlin for early and continuing sharing of analytic insights, and to J.C. Eilbeck and J.M. Hyman for independent verification of some critical numerical results. We are also very grateful to A. Bishop, E. Eichten, S. Gorenstein, J. Hills, S. Kivelson, J. Negele, M. Rice, H. Segur, S. Tremaine, S. Trullinger, D. Wilkinson, and C. Zachos for helpful conversations and remarks. One of us (J.S.) wishes also to thank the Center for Nonlinear Studies at the Los Alamos National Laboratory for its hospitality.

Appendix A

The numerical method

The numerical scheme used to solve eq. (1.4) was a simple finite difference technique. The field vari-

able $\phi(x, t)$ is discretized in space and time and is represented by ϕ_i^n where i is the spatial index and n is the temporal index. The numerical step sizes are denoted by Δx and Δt. Then to second order eq. (1.4) becomes

$$\frac{\phi_i^{n+1} - 2\phi_i^n + \phi_i^{n-1}}{\Delta t^2} - \frac{\phi_{i+1}^n - 2\phi_i^n + \phi_{i-1}^n}{\Delta x^2} - \phi_i^n + (\phi_i^n)^3 = 0 . \tag{A.1}$$

This is easily solved for ϕ_i^{n+1} in terms of previously calculated quantities.

This method is stable for $\Delta t < \Delta x$ (Courant condition). We found that the results converged for step sizes ≈ 0.01 and for most of the numerical work the step sizes were $\Delta x = 0.01$, $\Delta t = 0.009$. Further discussions of numerical accuracy can be found in ref. 28.

The starting function needed for this work is a widely separated kink and antikink moving towards each other with velocity v. This supplied $\phi(x, t = 0)$ and $\phi(x, t = \Delta t)$, i.e., the first two rows needed for eq. (A.1). The precise definition of the starting function is

$$\phi_0(x, t) = \tanh \frac{\gamma}{\sqrt{2}}(x + vt - x_0) - \tanh \frac{\gamma}{\sqrt{2}}(x - vt + x_0) + 1 ,$$
$$\gamma \equiv 1/\sqrt{1 - v^2} . \tag{A.2}$$

For this work the initial distance from the origin (x_0) was set at 7.0. Discussions of variations in x_0 can be found in ref. 28.

One difficulty with solving the ϕ^4 equation numerically is that energy given off during the $K\bar{K}$ interaction will propagate to the edge of the numerical grid, be reflected and eventually reach the center again. Given the delicate interplay between shape mode oscillations and translational motion, even small amounts of reflected energy could alter the results. Some thought was given to schemes for damping the oscillations at the grid boundaries thus eliminating reflections. Such schemes, however, seemed to be only partially effective and were discarded. The method used in this work to eliminate reflections was simply to make the grid large enough so that during the times of interest reflections could not get back to the center. The price for this was a large increase in computational time and memory. (A factor of 2 can be gained by shrinking the grid with the light cone as time advances.)

Since table I is the main numerical result in this work, the numerics leading to its generation should be discussed in more detail. As indicated above, the step sizes used were $\Delta x = 0.01$ and $\Delta t = 0.009$ with an initial kink distance from the center of $x_0 = 7$. The runs were made for a time $T = 300$ after the first $K\bar{K}$ collision. This is a critical parameter since for some initial velocities a $K\bar{K}$ capture can be mistaken for a bounce followed by escape if T is too short. A larger T would have been desirable but because of the boundary conditions the computational time and memory requirements go as T^2, thus making larger times with the above Δx and Δt impractical. Great care was taken to make certain that no reflection windows were missed in the velocity range studied ($v < 0.2555$). For low v where the windows are fairly large $\Delta v = 0.001$ was used to scan for the windows while $\Delta v = 0.0001$ was used to determine more precisely the window boundaries. At higher v the scan was made with $\Delta v = 0.0001$. In total the calculations for table I used about 20 hours of Cray-1 CPU time. The critical velocity v_c ($= 0.2598$) was determined with these same numerical parameters and $\Delta v = 0.0001$.

The velocity region $0.2555 < v < v_c$ has been largely ignored in this work. In order to resolve the very narrow windows in this region velocity scans with $\Delta v = 10^{-5}$ and smaller would have to be used. While possible this would, however, consume large quantities of computer time. It would be interesting to determine if the windows continue indefinitely or stop at some well-defined point that is *not* an artifact of the numerical scheme and/or computer time limitations.

Appendix B

The kink/anti-kink potential and collective coordinates

In section 3 we introduced an effective potential, $V(x_0)$, for the interaction between kink and antikink as a function of their separation, $2x_0$. We also described the relative motion of the bound $K\bar{K}$ pair by considering x_0 as a function of time and integrating explicitly the large separation form of the equations of motion for x_0. The fundamental approximation involved in this calculation is the replacement of the (infinitely) many degrees of freedom of a kink in the continuum field theory by a single "collective coordinate," x_0, which describes the gross features of the kink motion. In this appendix we discuss first the background technical details for the calculations of section 3 and then the more general problems involved in using collective coordinates to describe kink motions.

Following previous calculations [25, 30, 32] we define the $K\bar{K}$ potential as the total energy of a static field configuration of the form in (3.1). Explicitly, we shall consider the *Ansatz* function

$$\phi_A(x; x_0, y_0) \equiv \left[1 - \tanh\frac{y_0}{\sqrt{2}}(x + x_0) + \tanh\frac{y_0}{\sqrt{2}}(x - x_0)\right], \tag{B.1}$$

where for purposes of our later discussion we have slightly generalized the form in (3.1) to allow for a change of scale (y_0) for the kink and antikink. Only the special case $y_0 = 1$ is of direct relevance to section 3.

The energy in this static field configuration – which, of course, is *not* a solution to the full field equation (1.4) except for $y_0 = 1$ and in the limit $x_0 \to \infty$ – can be evaluated as a function of x_0 and y_0 by performing the integration indicated in (1.5).

One finds, for x_0 and y_0 considered as time-independent parameters,

$$V(x_0, y_0) \equiv \int dx \left[\frac{1}{2}\left(\frac{\partial\phi_A}{\partial x}\right)^2 + \frac{1}{4}(\phi_A^2 - 1)^2\right] \equiv V_1(x_0, y_0) + V_2(x_0, y_0), \tag{B.2}$$

with

$$\begin{aligned} V_1(x_0, y_0) &\equiv \int dx \frac{1}{2}\left(\frac{\partial\phi_A}{\partial x}\right)^2 \\ &= \frac{y_0^2}{4}\int dx \left[\operatorname{sech}^4\frac{y_0}{\sqrt{2}}(x + x_0) + \operatorname{sech}^4\frac{y_0}{\sqrt{2}}(x - x_0)\right. \\ &\quad \left. - 2\operatorname{sech}^2\frac{y_0}{\sqrt{2}}(x + x_0)\operatorname{sech}^2\frac{y_0}{\sqrt{2}}(x - x_0)\right] \end{aligned} \tag{B.3a}$$

and

$$\begin{aligned} V_2(x_0, y_0) &\equiv \int dx \frac{1}{4}(\phi_A^2 - 1)^2 \\ &= \frac{\tanh\sqrt{2}y_0x_0}{\operatorname{sech}\sqrt{2}y_0x_0}\int dx \operatorname{sech}^2\frac{y_0}{\sqrt{2}}(x + x_0)\operatorname{sech}^2\frac{y_0}{\sqrt{2}}(x - x_0) \\ &\quad \times \left\{1 - \frac{\tanh\sqrt{2}y_0x_0}{2\operatorname{sech}\sqrt{2}y_0x_0}\operatorname{sech}^2\frac{y_0}{\sqrt{2}}(x + x_0)\operatorname{sech}^2\frac{y_0}{\sqrt{2}}(x - x_0)\right\}^2. \end{aligned} \tag{B.3b}$$

In deriving (B.3b) we have used the identity

$$\operatorname{sech}\sqrt{2}y_0x_0\left[\tanh\frac{y_0}{\sqrt{2}}(x+x_0)-\tanh\frac{y_0}{\sqrt{2}}(x-x_0)\right]$$
$$=\tanh\sqrt{2}y_0x_0\operatorname{sech}\frac{y_0}{\sqrt{2}}(x+x_0)\operatorname{sech}\frac{y_0}{\sqrt{2}}(x-x_0)\,. \tag{B.4}$$

The integrals in (B.3) can be expressed as the $k=0$ limit of Fourier transforms which can be evaluated by contour integration. We skip the details and simply quote the results that

$$V_1(x_0,y_0)=\sqrt{2}y_0\left[\frac{2}{3}-\frac{2\operatorname{sech}^2\sqrt{2}y_0x_0}{\tanh^3\sqrt{2}y_0x_0}(\sqrt{2}y_0x_0-\tanh\sqrt{2}y_0x_0)\right] \tag{B.5a}$$

and

$$V_2(x_0,y_0)=\frac{\sqrt{2}}{y_0}\left[\frac{4}{\tanh\sqrt{2}y_0x_0}(\sqrt{2}y_0x_0-\tanh\sqrt{2}y_0x_0)\right.$$
$$-\frac{4}{\tanh^2\sqrt{2}y_0x_0}\{(3-\tanh^2\sqrt{2}y_0x_0)\sqrt{2}y_0x_0-3\tanh\sqrt{2}y_0x_0\} \tag{B.5b}$$
$$\left.+\frac{2}{\tanh^3\sqrt{2}y_0x_0}\{(5-3\tanh^2\sqrt{2}y_0x_0)\sqrt{2}y_0x_0+\frac{4}{3}\tanh^3\sqrt{2}y_0x_0-5\tanh\sqrt{2}y_0x_0\}\right].$$

These results are in agreement with the previous calculations in the literature [30, 32]. From (B.3) and (B.4) one can evaluate the asymptotic form of $V(x_0)$ for $x_0\to\infty$. For arbitrary y_0, one finds

$$V(x_0,y_0)\underset{x_0\to\infty}{\simeq}\sqrt{2}\left(\frac{2}{3}\left(y_0+\frac{1}{y_0}\right)+8\,\mathrm{e}^{-2\sqrt{2}y_0x_0}\left[\left(y_0-\frac{2}{y_0}\right)-\sqrt{2}y_0x_0\left(y_0-\frac{1}{y_0}\right)\right]\right), \tag{B.6a}$$

so that for the undeformed static kink/antikink pair, $y_0=1$,

$$V(x_0,1)\underset{x_0\to\infty}{\simeq}\sqrt{2}\left[\frac{4}{3}-8\,\mathrm{e}^{-2\sqrt{2}x_0}\right]. \tag{B.6b}$$

Recalling that the kink mass, M, in our (dimensionless) units is $M=2\sqrt{2}/3$, we see that $V(\infty,1)=2M$, so that $\tilde{V}(x_0)$ defined in the text is indeed given by (3.3).

If we allow x_0 and – again for purposes of our later discussion – y_0 to be functions of time, then (1.5) leads to an effective Hamiltonian describing the (coupled) motion of the now time-dependent parameters $x_0(t)$ and $y_0(t)$. The potential energy term in the effective Hamiltonian is just that given by (B.2)–(B.4). The kinetic energy term is defined by

$$T(x_0,y_0)\equiv\int\mathrm{d}x\,\frac{1}{2}\left(\frac{\partial\phi_{\mathrm{A}}}{\partial t}\right)^2, \tag{B.7a}$$

where

$$\frac{\partial\phi_{\mathrm{A}}}{\partial t}\equiv\frac{\partial\phi_{\mathrm{A}}}{\partial x_0}\dot{x}_0+\frac{\partial\phi_{\mathrm{A}}}{\partial y_0}\dot{y}_0\,. \tag{B.7b}$$

One finds

$$T(x_0, y_0) \equiv \frac{m_1(x_0, y_0)}{2}\dot{x}_0^2 + m_2(x_0, y_0)\dot{x}_0\dot{y}_0 + \frac{m_3}{2}(x_0, y_0)\dot{y}_0^2, \tag{B.7}$$

where

$$\begin{aligned} m_1(x_0, y_0) &= \frac{y_0^2}{2}\int_{-\infty}^{\infty} dx(\operatorname{sech}^4\sqrt{2}y_0(x + x_0) + \operatorname{sech}^4\sqrt{2}y_0(x - x_0) \\ &\quad + 2\operatorname{sech}^2\sqrt{2}y_0(x + x_0)\operatorname{sech}^2\sqrt{2}y_0(x - x_0)) \\ &= \sqrt{2}y_0\left[\frac{4}{3} + \frac{8\operatorname{sech}^2\sqrt{2}y_0x_0}{\tanh^3\sqrt{2}y_0x_0}(\sqrt{2}y_0x_0 - \tanh\sqrt{2}y_0x_0)\right], \end{aligned} \tag{B.8a}$$

$$\begin{aligned} m_2(x_0, y_0) &= \frac{x_0y_0}{2}\int_{-\infty}^{\infty} dx\ 2\operatorname{sech}^2\sqrt{2}y_0(x + x_0)\operatorname{sech}^2\sqrt{2}y_0(x - x_0) \\ &= \sqrt{2}x_0\left[\frac{4\operatorname{sech}^2\sqrt{2}y_0x_0}{\tanh^3\sqrt{2}y_0x_0}(\sqrt{2}y_0x_0 - \tanh\sqrt{2}y_0x_0)\right], \end{aligned} \tag{B.8b}$$

and

$$\begin{aligned} m_3(x_0, y_0) &= \tfrac{1}{2}\int dx[(x + x_0)^2\operatorname{sech}^4\sqrt{2}y_0(x + x_0) + (x - x_0)^2\operatorname{sech}^4\sqrt{2}y_0(x - x_0) \\ &\quad - 2(x^2 - x_0^2)\operatorname{sech}^2\sqrt{2}y_0(x + x_0)\operatorname{sech}^2\sqrt{2}y_0(x - x_0)] \\ &= \frac{2\sqrt{2}}{3y_0^3}\left\{2\left(\frac{\pi^2}{6} - 1\right) - \frac{\operatorname{sech}^2\sqrt{2}y_0x_0}{\tanh^3\sqrt{2}y_0x_0}(\pi^2(\sqrt{2}y_0x_0 - \tanh\sqrt{2}y_0x_0) - 4\sqrt{2}y_0x_0)\right\}. \end{aligned} \tag{B.8c}$$

The integrals in (B.8c) can be evaluated by taking derivatives with respect to k (at $k = 0$) of the same Fourier transforms which were used to evaluate (B.3).

In section 3, only the form of the kinetic energy for $y_0 = 1$ (and constant in time) in required, and thus only $m_1(x_0, 1)$ is relevant. Recalling $M = 2\sqrt{2/3}$, we see that

$$m_1(x_0, 1) = 2M + 2I(x_0), \tag{B.9a}$$

where

$$I(x_0) = 4\sqrt{2}\frac{\operatorname{sech}^2\sqrt{2}x_0}{\tanh^3\sqrt{2}x_0}(\sqrt{2}x_0 - \tanh\sqrt{2}x_0). \tag{B.9b}$$

Hence the kinetic energy term appropriate for the discussion of section 3 is, as indicated in (3.2),

$$T = M\dot{x}_0^2 + I(x_0)\dot{x}_0^2,$$

where $I(x_0)$ vanishes exponentially as $x_0 \to \infty$, as asserted in the text.

With these technical details established, we turn next to our general discussion of the use of collective coordinates to describe kink motion [19, 25, 30, 32, 42]. For simplicity, let us start at an intuitive level by recalling that our whole approach to the resonance phenomenon rested on isolating two (of the infinitely many) degrees of freedom for each of the antikink/kink pair: namely, the rigid translational motion and the shape oscillation. Clearly these are coordinates being used to describe collective motions and are thus, at a practical level, "collective coordinates" for the kink and antikink. To understand these collective coordinates in more detail, we can start by focussing on the case of a single kink and recalling (see section 2) that in the small oscillations around the kink solution there are two discrete modes which correspond directly to our two coordinates. One, with characteristic frequency $\omega = 0$, corresponds to the infinitesimal translations of the kink. The second, with $\omega = \sqrt{3/2}$, represents a localized deformation of the kink shape. Although we have argued that both can be thought of as collective coordinates, there is a very important distinction between them. Since the ϕ^4 equation in (1.4) is translationally invariant in space, the energy of a single kink – obtained by inserting (1.6) into (1.5) – is independent of the location of the kink [x_0 in (1.6)]. As a consequence of this invariance, in the expansion around the kink one finds a mode with $\omega = 0$; in particle physics language, this is the "Goldstone mode" arising from the breaking of the translational invariance of the theory that occurs by placing the kink at a definite location [44, 45]. Because it is related to a symmetry of the equation, the collective coordinate corresponding to this mode is a "strict" collective coordinate in the sense that it can not be treated simply by linearly superposing the corresponding eigenfunction (which is the spatial derivative of the kink) with the kink itself. In classical perturbation theory, this would lead to a "secular" term: that is, a perturbation whose effect increases (in this case linearly) in time. In quantum fluctuation theory, this would lead to unbounded (i.e., infinite) fluctuations. The correct way to account [44, 45] for the translational degree of freedom of the kink is to do precisely what we did with only a heuristic motivation above: namely, allow the location of the kink, x_0, to become a time-dependent coordinate and determine its motion so as to eliminate secular perturbations or unbounded fluctuations. Thus, for the translational motion of a single kink, our heuristic collective coordinate approach can be made rigorous [44–47].

In the case of the shape mode at $\omega_s = \sqrt{3/2}$, there is no associated symmetry, and hence it can be termed an "approximate" collective coordinate. Isolating it from among all the other degrees of freedom is based on the physical and intuitive arguments given in the text. It remains an interesting, open problem to understand rigorously the role of this discrete mode in full, nonlinear perturbation theory around the kink [46].

All of the above remarks on collective coordinates have appled to the case of a single kink. In our application to $K\bar{K}$ scattering, the effective replacement of the kink and antikink by their translational and shape deformation degrees of freedom is always an approximation. In particular, the coordinate $2x_0$ in (3.1) or (B.1), which represents the *separation* between the kink and antikink, does *not* correspond to any underlying symmetry of the equation; an easy way to see this is to note that the energy corresponding to the field configuration in (3.1) or (B.1) is a strong function of x_0.

The reason our approximate approach works so well for $K\bar{K}$ scattering appears to be, as indicated in the text, the existence of a long interval between the first and second $K\bar{K}$ collisions during which the kinks are effectively separated and acting only as perturbations on each other.

To conclude this discussion of collective coordinates we should mention a recent alternative formulation [19, 42, 48, 49] in which the effects of the shape mode oscillation, rather than being linearly superposed as in our approach, are incorporated parametrically directly in the kink waveform. This approach has been used to describe the coupling of shape oscillations and translations of solitons, perturbed by external radiation, in a model of polyacetylene [19, 42]. In our discussion at the beginning of this appendix, this

method is illustrated by the introduction of y_0 in (B.1). To distinguish these two approaches, let us refer to the first as the "linear eigenfunction collective coordinate" (LECC) approach and the second as the "parametric collective coordinate" (PCC) approach.

To understand the general features of the PCC approach, as well as its relation to the LECC method, it is useful to start with the case of a single kink, for which the PCC Ansatz including translational and shape degrees of freedom is

$$\phi_A(x; x_0(t), y_0(t)) = \tanh \frac{y_0(t)(x - x_0(t))}{\sqrt{2}}. \tag{B.10}$$

Clearly, by substituting this expression into (1.5) and using (B.6b) to evaluate the time derivative, one can obtain an effective Hamiltonian for the collective coordinates x_0 and y_0. Before doing this, let us first observe the relation between the PCC and LECC that follows by considering the form of (B.10) for static x_0 and y_0 and for y_0 near its value for a true solution to (1.4), $y_0 = 1 + \epsilon$. Expanding in powers of ϵ, one sees

$$\phi_A(x; x_0, y_0 = 1 + \epsilon) = \tanh\left(\frac{x - x_0}{\sqrt{2}}\right) + \frac{\epsilon}{\sqrt{2}}(x - x_0)\,\mathrm{sech}^2\frac{(x - x_0)}{\sqrt{2}} + \mathcal{O}(\epsilon^2). \tag{B.11}$$

Thus, at this level, the PCC approach amounts to approximating the true linear eigenfunction corresponding to the shape mode,

$$\delta\phi_s \propto \mathrm{sech}\frac{(x - x_0)}{\sqrt{2}} \tanh\frac{(x - x_0)}{\sqrt{2}} \tag{B.12}$$

by

$$(\delta\phi_s)_A \propto (x - x_0)\,\mathrm{sech}^2\left(\frac{x - x_0}{\sqrt{2}}\right). \tag{B.13}$$

Clearly, these functions are qualitatively similar for $x \simeq x_0$ but differ quantitatively, particularly in their rate of exponential falloff as $x - x_0 \to \infty$. Note that this comparison, apart from showing the qualitative similarity, also shows that the PCC Ansatz, unlike the LECC form, is not exact to $\mathcal{O}(\epsilon^1)$. This makes any direct attempt to put this approach on more rigorous footing difficult [46].

If one nonetheless pursues the PCC approach, one finds that it leads to an interesting, closed coupled system of equations for $x_0(t)$ and $y_0(t)$. These can be derived from the effective Hamiltonian obtained by substituting (B.11) into (1.5). Alternatively, one can simply take the $x_0 \to \infty$ limit of the expressions in (B.2)–(B.8), and divide by two since they refer to the kink plus antikink configuration (B.1). Either way, one finds [19, 42, 48, 49]

$$H_{\mathrm{eff}}(x_0, y_0) = \frac{\sqrt{2}}{3} y_0 \dot{x}_0^2 + \frac{\sqrt{2}}{3}\left(\frac{\pi^2}{6} - 1\right)\frac{\dot{y}_0^2}{y_0^3} + \frac{\sqrt{2}}{3}\left(y_0 + \frac{1}{y_0}\right). \tag{B.14}$$

From this effective Hamiltonian one obtains the equations

$$\frac{\mathrm{d}}{\mathrm{d}t}(\dot{x}_0 y_0) = 0, \quad \text{so } \dot{x}_0 y_0 = \text{constant} \equiv \alpha \tag{B.15a}$$

and

$$\beta\left[\frac{\ddot{y}_0}{y_0^3}-\frac{3}{2}\frac{\dot{y}_0^2}{y_0^4}\right]+\frac{1}{2}\left(1-\frac{(1+\alpha^2)}{y_0^2}\right)=0\,, \tag{B.15b}$$

where $\beta \equiv \pi^2/6 - 1$.

It is easy to see that these PCC equations admit the solution $\dot{x}_0 = v$, $y_0 = (1-v^2)^{-1/2}$, which corresponds to the rigidly translating, Lorentz-contracted kink which is an *exact* solution to the full equation (1.4). With a bit more analysis, one can show that eq. (B.15) admits an exact time-dependent solution, in which [48, 49]

$$y_0 = \alpha/\dot{x}_0 \tag{B.16a}$$

and

$$\dot{x}_0 = \frac{\alpha}{\sqrt{\alpha^2+1}}(\alpha + \sqrt{\alpha^2-1}\sin\omega t)\,, \tag{B.16b}$$

with $\omega^2 = (1+\alpha^2)/\beta$.

In terms of the full equation, this solution would correspond to a "wobbling" and translating isolated kink. Of course, one can show directly that using this solution in the Ansatz (B.10) does *not* produce an exact solution to the full field equation (1.4). Nonetheless, it does raise an interesting question concerning the possible existence of a wobbling kink solution to ϕ^4. Clearly, this deserves further investigation.

An important aspect of this question, particularly from the perspective of comparing the PCC and LECC approaches, is that the PCC Ansatz would lead to no natural distinction between the ϕ^4 and sine-Gordon equations. Specifically, if one took for a sine-Gordon kink an Ansatz comparable to (B.10),

$$u_A(x; x_0(t), y_0(t)) = 4\tan^{-1} e^{y_0(t)(x-x_0(t))}\,, \tag{B.17}$$

one would obtain coupled equations for x_0 and y_0 of precisely the same form as (B.15), with slightly different constants. Yet in the LECC approach, one finds immediately that in the small oscillations around the sine-Gordon kink, the only localized mode is the translation mode at $\omega = 0$; there is no discrete mode corresponding to a shape oscillation. In essence, the PCC approach implies that modes from the continuum can play the role of the shape oscillation and, just as in ϕ^4, lead to a wobbling kink. Although much further study is needed in this context as well, there are several potential problems with this result. First, at a rigorous level, using perturbation theory with inverse scattering techniques (which can be applied because the unperturbed sine-Gordon equation is integrable), one can show that the asymptotic form of perturbed sine-Gordon kink can not wobble [50]. Second, at a phenomenological level, the calculations of $K\bar{K}$ collisions in the modified sine-Gordon equation [39] show that there does appear to be a striking distinction between the cases in which a discrete shape mode is present and those in which it is not; in the former one finds resonances in the scattering, in the latter one doesn't. Thus it seems important to pursue the comparative study of the PCC and LECC approaches to clarify this and related questions.

References

[1] For a variety of recent reviews see Solitons in Condensed Matter Physics, A.R. Bishop and T. Schneider, eds. (Springer, Berlin, 1978). Physics in One Dimension, J. Bernasconi and T. Schneider, eds. (Springer, Berlin, 1981). Solitons in Action, K. Lonngren and A.C. Scott, eds. (Academic Press, New York, 1978). Physica Scripta 20 (1979) 291–562. S. Coleman, in: New Phenomena in Sub-

nuclear Physics, A. Zichichi, ed. (Plenum, New York, 1977). R.K. Bullough and P.J. Caudrey, Solitons (Springer, Berlin, 1980).
[2] The classic review remains A.C. Scott, F.Y.F. Chu and D.W. McLaughlin, Proc. IEEE 61 (1973) 1443.
[3] For a review of dynamics of solitary waves in non-integrable systems, see V.G. Makhankov, Phys. Repts. 35 (1978) 1.
[4] For an example of recent rigorous results in the area and some earlier references, see J.-M. Coron, Compt. Rend. Acad. Sc. Paris V. 1 294 Series I, (1982) 127.
[5] V.N. Ginzburg and L.D. Landau Zh. Exsp. Teor. Fiz. 20 (1950) 1064 (in Russian); discussed at length in A.L. Fetter and J.D. Walecka, Quantum Theory of Many-Particle Systems (McGraw-Hill, New York, 1971).
[6] For reviews see R.A. Cowley, Adv. in Phys. 29 (1980) 1. A.D. Bruce, Adv. in Phys. 29 (1980) 111; A.D. Bruce and R.A. Cowley, Adv. in Phys 29 (1980) 219.
[7] Y. Ishibashi and Y. Takagi, J. Phys. Soc. Japan 33 (1972) 1.
[8] S. Aubry and R. Pick, Ferroelectrics 8 (1979) 471.
[9] S. Aubry, J. Chem. Phys. 64 (1975) 3217.
[10] S. Aubry, J. Chem. Phys. 64 (1976) 3392.
[11] J.A. Krumhansl and J.R. Schrieffer, Phys. Rev. B. 11 (1975) 3535.
[12] C.M. Varma, Phys. Rev. B14 (1976) 244.
[13] T. Schneider and E. Stoll, Phys. Rev. Lett. 35 (1975) 296.
[14] T.R. Koehler, A.R. Bishop, J.A. Krumhansl and J.R. Schrieffer, Solid State Communications 17 (1975) 1515.
[15] Y. Wada and J.R. Schrieffer, Phys. Rev. B18 (1978) 3897.
[16] G.M. Mazenko and P.S. Sahni, Phys. Rev. B18 (1978) 6139; P.S. Sahni and G.F. Mazenko, Phys. Rev. B20 (1979) 4674.
[17] J.F. Currie, J.A. Krumhansl, A.R. Bishop and S.E. Trullinger, Phys. Rev. B22 (1980) 477.
[18] M.J. Rice, Phys. Lett 71A (1979) 153; M.J. Rice and J. Timonen, Phys. Lett. 73A (1979) 368.
[19] M.J. Rice and E.J. Mele, Solid State Commun. 35 (1980) 487.
[20] W.P. Su, J.R. Schrieffer and A.J. Heeger, Phys. Rev. Lett. 42 (1979) 1698; Phys. Rev. B22 (1980) 2099. H. Takayama, Y.R. Lin-liu and K. Maki, Phys. Rev. B21 (1980) 2388. R. Jackiw and J.R. Schrieffer, Nucl. Phys. B190 [F53] (1981) 253.
[21] R.F. Dashen, B. Hasslacher and A. Neveu, Phys. Rev. D10 (1974) 4130; Phys. Rev. D11 (1975) 3424. J. Goldstone and R. Jackiw, Phys. Rev. D11 (1975) 1486. R. Rajaraman, Phys. Repts. 21 (1975) 229.
[22] D.K. Campbell and Y.T. Liao, Phys. Rev. D14 (1976) 2093; D.K. Campbell, in: Nuclear Physics with Heavy Ions and Mesons, Les Houches Session XXX, R. Balian, M. Rho and G. Ripka, eds. (North-Holland, Amsterdam, 1978), p. 674.
[23] R. Jackiw and C. Rebbi, Phys. Rev. D13 (1976) 3398.
[24] S. Weinberg, Phys. Rev. Lett. 19 (1967) 1264. A. Salam, Elementary Particle Theory Relativistic Groups and Analyticity (Nobel Symposium No. 8) N. Svartholm, ed. (Almquist and Wiksell, Stockholm, 1968). For a recent review, see H. Fritzsch and P. Minkowski, Phys. Repts. 73 (1981) 67.
[25] A.E. Kudryavtsev, JETP Lett. 22 (1975) 82.
[26] B.S. Getmanov, JETP Lett. 24 (1976) 291.
[27] V.G. Makhankov, Phys. Repts. 35C (1978) 1.
[28] C.A. Wingate, Ph.D. Thesis, University of Illinois (1978); and SIAM J. Appl. Math. 43 (1983) 120.
[29] M.J. Ablowitz, M.D. Kruskal and J.R. Ladik, SIAM J. Appl. Math. 36 (1979) 478.
[30] T. Sugiyama, Prog. Theor. Phys. 61 (1979) 1550.
[31] R. Klein, W. Hasenfratz, N. Theodorakopoulos and W. Wünderlich, Ferroelectrics 26 (1980) 721.
[32] M. Moshir, Nucl. Phys. B185 (1981) 318.
[33] J.K. Perring and T.H.R. Skyrme, Nuc. Phys 31 (1962) 550.
[34] One should resist the temptation to conclude that, simply because the kinks cannot pass through each other, they can *not* be solitons. One can imagine a purely elastic reflection and indeed, this is the case for kink/antikink scattering in the (completely integrable) "classical Gross–Neveu model." See A. Neveu and N. Papanicolaou, Commun. Math. Phys. 58 (1978) 31.
[35] W. Hasenfratz and R. Klein, Phy. 89A (1977) 191.
[36] P.M. Morse and H. Feshbach, Methods of Theoretical Physics, vol. II (McGraw-Hill, New York, 1953).
[37] Such three bounce windows have been observed in numerical simulations in a modified sine-Gordon model. M. Peyrard and D.K. Campbell, Physica 9D (1983) 33 (next paper).
[38] P. Bonche, S. Koonin and J.W. Negele, Phys. Rev. C13 (1976) 1226. See in particular the discussion of fig. 10 of this reference.
[39] M. Peyrard and D. Campbell, Physica 9D (1983) 33 (next paper).
[40] M. Peyrard and M. Remoissenet, Phys. Rev. B 26 (1982) 2886; M. Remoissenet and M. Peyrard, J. Phys. C14 (1981) L481.
[41] Work in this direction is currently in progress (D.W. McLaughlin and H. Segur, private communications).
[42] M.J. Rice, Phys. Rev. B24 (1981) 3638; in Nonlinear Problems, Present and Future, A.R. Bishop, D. K. Campbell and B. Nicolaenko, eds. (North-Holland, Amsterdam, 1982), p. 189.
[43] M. Nakahara and K. Maki, Phys. Rev. B25 (1982) 7789.
[44] J.L. Gervais and B. Sakita, Phys. Rev. D11 (1975) 2943. E. Tomboulis, Phys. Rev. D12 (1975) 1678.
[45] For a series of relevant papers on this topic, see Physics Reports 23C (1975) 237 (J.L. Gervais and A. Neveu, eds.).
[46] D. McLaughlin and M. Segur, private communications.
[47] In particular, although it is not obvious from our discussion, the approach can be made completely consistent with Lorentz invariance. See refs. 44 and 45.
[48] M.J. Rice, Phys. Rev. B, to be published.
[49] D.K. Campbell, unpublished.
[50] H. Segur, J. Math. Phys. 24 (1983) 1439.